

# Brackish groundwater desalination by constant current membrane capacitive deionization (MCDI): Results of a long-term field trial in Central Australia

Yunyi Zhu<sup>a,b</sup>, Christopher Miller<sup>b</sup>, Boyue Lian<sup>b</sup>, Yuan Wang<sup>a,b</sup>, John Fletcher<sup>c</sup>, Hang Zhou<sup>c</sup>, Zhizhao He<sup>a,b</sup>, Shunzhi Lyu<sup>a</sup>, Megan Purser<sup>d</sup>, Peter Juracich<sup>d</sup>, David Sweeney<sup>d</sup>, T. David Waite<sup>a,b,\*</sup>

<sup>a</sup> UNSW Centre for Transformational Environmental Technologies (CTET), Yixing, Jiangsu, China

<sup>b</sup> Water Research Centre, School of Civil and Environmental Engineering, UNSW Sydney, Australia

<sup>c</sup> School of Electrical Engineering and Telecommunications, UNSW Sydney, Australia

<sup>d</sup> Power and Water Corporation, Northern Territory, Australia

## ARTICLE INFO

### Keywords:

Membrane capacitive deionization (MCDI)

Long-term performance assessment

Electrode regeneration

Portable water treatment

Water-energy nexus

## ABSTRACT

A long-term field trial of membrane capacitive deionization (MCDI) was conducted in a remote community in the Northern Territory of Australia, with the aim of producing safe palatable drinking water from groundwater that contains high concentrations of salt and hardness ions and other contaminants. This trial lasted for 1.5 years, which, to our knowledge, is one of the longest reported studies of pilot-scale MCDI field trials. The 8-module MCDI pilot unit reduced salt concentration to below the Australian Drinking Water Guideline value of 600 mg/L total dissolved solids (TDS) concentration with a relatively high water recovery of  $71.6 \pm 8.7\%$ . During continuous constant current operation and electrode discharging at near zero volts, a rapid performance deterioration occurred that was primarily attributed to insufficient desorption of multivalent ions from the porous carbon electrodes. Performance could be temporarily recovered using chemical cleaning and modified operating procedures however these approaches could not fundamentally resolve the issue of insufficient electrode performance regeneration. Constant current discharging of the electrodes to a negative cell cut-off voltage was hence employed to enhance the stability and overall performance of the MCDI unit during the continuous operation. An increase in selectivity of monovalent ions over divalent ions was also attained by implementing negative voltage discharging. The energy consumption of an MCDI system with a capacity of 1000 m<sup>3</sup>/day was projected to be 0.40~0.53 kWh/m<sup>3</sup>, which is comparable to the energy consumption of electrodialysis reversal (EDR) and brackish water reverse osmosis (BWRO) systems of the same capacity. The relatively low maintenance requirements of the MCDI system rendered it the most cost-efficient water treatment technology for deployment in remote locations. The LCOW of an MCDI system with a capacity of 1000 m<sup>3</sup>/day was projected to be AU \$1.059/m<sup>3</sup> and AU\$1.146/m<sup>3</sup> under two operational modes, respectively. Further investigation of particular water-energy trade-offs amongst MCDI performance metrics is required to facilitate broader application of this promising water treatment technology.

## 1. Introduction

Availability of water suitable for domestic and agricultural purposes is an increasing global challenge that affects over 2 billion people in today's world, especially in Australia where water resources of acceptable quality are becoming less available due to extreme drought events and climate change ([Australian Government Geoscience Australia, 2023; World Health Organization, 2024](#)).

For many remote communities in central Australia, groundwater is often the only reliable source of potable water. However, it can be brackish and contain high levels of contaminants that exceed the Australian Drinking Water Guideline (ADWG) values ([National Health and Medical Research Council, 2011](#)). Water purification and desalination is hence required to reduce the total dissolved solids (TDS) concentration to below the ADWG value of 600 mg/L TDS and remove other contaminants, including uranium in some

\* Corresponding author.

E-mail address: [d.waite@unsw.edu.au](mailto:d.waite@unsw.edu.au) (T.D. Waite).

<b>Nomenclature</b>	
<b>Abbreviation</b>	
ADWG	Australian drinking water guideline
AEM	Anion exchange membrane
BWRO	Brackish water reverse osmosis
CC	Constant current
CC-RCD	Constant current-reverse current discharge
CC-RCD-DNV	Constant current-reverse current discharge with the reversed current applied until the resulting cell voltage decreases to a pre-assigned negative cut-off voltage
CC-RCD-DPV	Constant current-reverse current discharge with the reversed current applied until the resulting cell voltage decreases to a pre-assigned positive cut-off voltage
CC-ZVD	Constant current-zero voltage discharge (short-circuiting discharge)
CDI	Capacitive deionization
CEM	Cation exchange membrane
CFA	Colorimetric flow analyser
CIP	Clean-in-place
CV	Constant voltage
CV-RVD	Constant voltage-reverse voltage discharge
DC	Direct current
EC	Electrical conductivity
ED	Electrodialysis
EDL	Electrical double layer
EDR	Electrodialysis reversal
ICP-AES	Inductively coupled plasma atomic emission spectrometry
IEM(s)	Ion exchange membrane(s)
ISE	Ion selective electrode
MCDI	Membrane capacitive deionization
O&M	Operation and maintenance
PLC	Programmable logic controller
RO	Reverse osmosis
SI	Supplementary information
TDS	Total dissolved solids
<b>Symbols</b>	
$\langle c_f \rangle$	Ion concentration in the feedwater
$\langle c_p \rangle$	Ion concentration in the product water
$\langle \Delta c \rangle$	Ion concentration reduction
$C_{Labour \& Travel}$	Cost of labour and relating travel for system services
$C_{O\&M}$	Annual O&M costs of different systems
$C_{equipment}$	Capital cost of a piece of equipment
$C_{general \ O\&M}$	Cost of general operation and maintenance activities
$EAC_{major}$	Equivalent annual capital cost of major components
$EAC_{others}$	Equivalent annual capital cost of other components
$E_{ancillary}$	Volumetric energy consumption of ancillary electrical systems
$E_{in}$	Total energy input to eight MCDI modules over one MCDI cycle
$E_{out}$	Total energy that can be recovered from eight MCDI modules over one MCDI cycle
$E_{pump}$	Volumetric energy consumption of pumps
$E_t$	Volumetric energy consumption of the MCDI system
$E_v$	Volumetric electrode energy consumption
$E_{valve}$	Volumetric energy consumption of valves
$V_b$	Generated brine volume of one MCDI module
$V_{p, \ annual}$	Annual production of the water treatment system
$V_p$	Product volume of one MCDI module
$i_r$	Rate charged on the loan for the capital cost or the discount rate
$\sigma_f$	Electrical conductivity of the feedwater
$\sigma_p$	Electrical conductivity of the product water
$\Delta t_b$	Duration of brine discharge
$\Delta t_{cycle,0}$	Cycle time of the first steady-state cycle after the restart of the unit operation during intermittent CC-RCD-DPV operation
$\Delta t_{cycle}$	Cycle time, total duration of one MCDI charging-discharging-idle cycle
$\Delta t_{down}$	Unit idle time, the time since the previous continuous CC-RCD-DPV operation ceased
$\Delta t_p$	Duration of product discharge
$\Delta EC$	Electrical conductivity reduction
$i \ and \ j$	Specific competing ions
LCOW	Levelized cost of water
$A$	Projected facial area of the MCDI cell
CRF	Capital recovery factor
$I$	Applied current
$P$	MCDI productivity
$Q$	Volumetric flowrate through one MCDI module
RE	Removal efficiency
$V$	Cell voltage
WR	Water recovery
$n$	Number of cells (electrode pairs) in one MCDI module
$t$	Expected lifetime of a piece of equipment
$\rho$	Ion selectivity

cases, to an acceptable level.

Pressure-driven reverse osmosis (RO) and electro-driven electrodialysis (ED) are the most accepted water desalination technologies. However, both treatment processes suffer severely from membrane scaling and fouling issues during long-term operation (Anderson et al., 2010), rendering them less energy and cost efficient, especially in continuously treating water with relatively low salt concentrations. Although periodic reversal of electrode polarity and switching of flow channels for the dilute and concentrate streams (a process known as electrodialysis reversal (EDR)) can effectively minimize the risk of scaling in traditional ED, it has been argued that the lifespan of the electrodes could be reduced by doing so (Sedighi et al., 2023). Capacitive deionization (CDI), a close cousin of ED, has recently gained increasing attention as a potentially viable alternate desalination technology due to its purported low energy consumption and high water recovery (Suss et al., 2015). An electric field is applied in CDI to polarize the electrode pairs. Salt ions of the opposite charge to the cathode/anode (termed counter-ions) are removed from water by

electrostatic attraction and temporarily stored within the electrical double layer (EDL) that is formed on the electrode surface (and within electrode pores). When the electrodes and their associated EDLs are saturated with ions, short-circuiting or a reversed current/voltage is applied to release the adsorbed ions from the EDL and regenerate the adsorption capacity of the electrodes without the need for additional chemicals. Nevertheless, ions carrying the same charge as the polarized electrode (termed co-ions) are repelled concurrently with counter-ion adsorption during the electrode charging process, known as co-ion expulsion, in conventional CDI, which unavoidably results in a reduction in salt adsorption capacity (Lee and Choi, 2012). By adding a layer of ion exchange membranes (IEMs) on the feed stream-facing surface of the CDI electrodes, the so-called membrane capacitive deionization (MCDI) process will prevent the occurrence of co-ion expulsion. The accessibility of oxygen to the electrodes can also be inhibited so that the Faradaic reactions will be greatly minimized in MCDI, thereby leading to an improved desalination performance compared to conventional CDI (Hassanvand et al., 2017; McNair et al., 2021; Tang et al., 2017).

Another significant advantage of MCDI is that a negative electrode cell voltage (known as polarity reversal) can be applied or reached during the electrode discharging process. In this case, the cations and anions that are released from the EDL during the electrode discharging step are electrostatically attracted to the (now) oppositely charged electrode but are prevented from reaching these electrodes as a result of the presence (at the surface of the electrodes) of IEMs of the same charge as the respective anions and cations. As a result, ion desorption can be more effective in recovering the electrode adsorption capacity for the subsequent electrode charging step (Biesheuvel and van der Wal, 2010; Yao and Tang, 2017). Furthermore, MCDI systems can be operated at a relatively low voltage compared to other electrified water treatment approaches, typically less than 1.6 V, making it compatible with use of photovoltaic cells and, as such, off-grid operation in remote and resource-constrained locations is possible (Tan et al., 2018; Zhang et al., 2013).

MCDI can be operated in either constant current (CC) or constant voltage (CV) mode. Although some studies suggest that CC operation might not be as energy efficient as CV operation (Dykstra et al., 2018), it is now generally recognized that CC operation is more advantageous than CV operation in real-world operations with more stable product quality during the electrode charging stage and facile energy recovery during the electrode discharging stage (He et al., 2021; Kang et al., 2014; Qu et al., 2016; Ramachandran et al., 2018; Wang and Lin, 2018). In CC operation, the electrodes can be either discharged by reversing the applied current flow (termed constant current-reverse current discharge (CC-RCD)) or short-circuiting the electrodes (termed constant current-zero voltage discharge (CC-ZVD)). Given that short-circuiting will cause a large peak in current which may overload associated electronic devices, current controlled electrode discharging is typically employed in large-scale MCDI operations.

Different flow modes have also been trialled in previous MCDI field studies. The brine stream generated from the electrode discharging step can be discharged under either continuous flow or stopped flow conditions. It has been shown that the stopped flow condition can provide a higher water recovery (of up to 85%) than that which can be achieved in continuous flow mode (He et al., 2021; Ramachandran et al., 2019; Tan et al., 2020). Recently, an operational-scale MCDI field trial employing CC-RCD operation and utilizing a stopped flow strategy for brine discharge successfully demonstrated the efficacy of applying MCDI in wastewater recycling (Bales et al., 2023).

So far, most of the studies relating to CC operation of MCDI systems have primarily focused on examining MCDI performance in relation to different operating parameters such as feed flowrate and applied current (Chen et al., 2018a; Porada et al., 2013; Sharan et al., 2021; Zhao et al., 2012a, 2013). However, the impact of different electrode discharging modes on the regeneration of electrode adsorption capacity has rarely been investigated, especially in long-term MCDI studies. Reversing the electrode polarity by discharging the electrodes to a negative cell cut-off voltage in CC operation (termed CC-RCD-DNV operation) can lead to improved electrode regeneration as previously elucidated, which is crucial in enabling the continuous operation of MCDI systems. From our reading of the literature, polarity reversal for electrode regeneration has only been thoroughly examined in CV mode via applying a reversed voltage (Biesheuvel et al., 2011; Porada et al., 2013; Shen et al., 2021; Zhao et al., 2012a). Although experiments on CC-RCD-DNV operation have already been undertaken by van Limpt and van der Wal (2014), Son et al. (2023) and Luong et al. (2023) in real-world operations such as cooling tower blowdown treatment and post-treatment of RO permeate, electrode regeneration and overall MCDI performance in CC-RCD-DNV has only been compared with other MCDI operational modes at laboratory scale studies by a few investigators. He et al. (2023) found that CC-RCD-DNV mode resulted in better electrode regeneration compared with other CC-RCD operational modes in which the cell cut-off voltage for the electrode discharging process was low positive volts (termed CC-RCD-DPV). However, the effect of operating in CC-RCD-DNV mode

on MCDI performance during long-term field operation has not been thoroughly investigated.

In this study, an eight-module pilot unit was deployed at a remote community in Central Australia. The MCDI performance, including productivity, water recovery and the efficacy in removal of specific inorganic ions, has been assessed over a trial period of 562 days. In particular, the stability of MCDI performance under CC-RCD-DPV and CC-RCD-DNV operational modes was examined to evaluate the efficacy of different electrode performance regeneration and maintenance approaches. Furthermore, a comparative assessment of energy consumption and operation and maintenance (O&M) costs of different brackish water treatment technologies was conducted to demonstrate the energy and economic efficiency of the MCDI system compared to EDR and RO systems for delivering treated potable water at remote locations.

## 2. Experimental

### 2.1. Setup of the containerized MCDI unit

After completion of initial testing and system rectification, the containerized unit was connected to the domestic water supply for a remote community of approximately 500 people in the Northern Territory of Australia. Fig. 1 depicts the general process flow of the MCDI groundwater treatment plant. The pilot-scale MCDI unit contributed around 2% of the required maximum demand ( $\sim 20 \text{ m}^3/\text{day}$  out of  $\sim 1000 \text{ m}^3/\text{day}$ ) of this remote community. The remaining potable water supply for this community was provided by a full-scale EDR unit (SUEZ 2020 EDR system, Veolia, Australia) that has been operating since 2013 and was operated in parallel with the MCDI unit throughout the trial.

As shown in Section S1 of the supplementary information (SI), the containerized MCDI unit consisted of eight commercial MCDI modules (IS CapDI module, Voltea, Netherlands) which were housed within a 20-foot standard shipping container. Each module contains 408 cells (electrode pairs) with a projected facial area of  $256 \text{ cm}^2$  per cell. During the unit operation, water was pumped from a raw water ground tank which was supplied by two groundwater bores. Around  $1\sim 2.4 \text{ m}^3/\text{h}$  feedwater was transferred into the MCDI system by a centrifugal pump and then filtered through a 5-micron cartridge filter to remove the majority of suspended particles before passing into individual MCDI electrode modules. As the feed groundwater contained relatively low level of metals, organics and turbidity (the complete water composition is listed later in Table 2), and was chlorinated before the raw water storage tank, no additional pre-treatment was required to further remove these contaminants that could otherwise potentially compromise the MCDI performance. The MCDI electrode modules were operated in a cyclical manner for groundwater desalination and electrode performance regeneration (as explained in the following section). In addition, all the MCDI modules were connected in parallel hydraulically and were operated in a “synchronized” mode in which the electrode charging (i.e., ion electro-adsorption) and discharging (i.e., ion electro-desorption) processes occurred simultaneously across each of the MCDI modules (though each MCDI module was electrically independent and could be operated separately if required). The treated product water was temporarily stored in a product water tank before being transferred out of the containerized unit and mixed with the EDR product water for domestic potable water supply, while the brine was directly discharged to an evaporation pond. Bi-directional DC-DC converters and a dedicated energy recovery system were incorporated in this MCDI water treatment system (Tan et al., 2020) and, in principle, could achieve an energy recovery of around 30%. The on-site and remote operation of the MCDI modules and other system equipment were automatically controlled by a Siemens s7-200 SMART series Programmable Logic Controller (PLC).

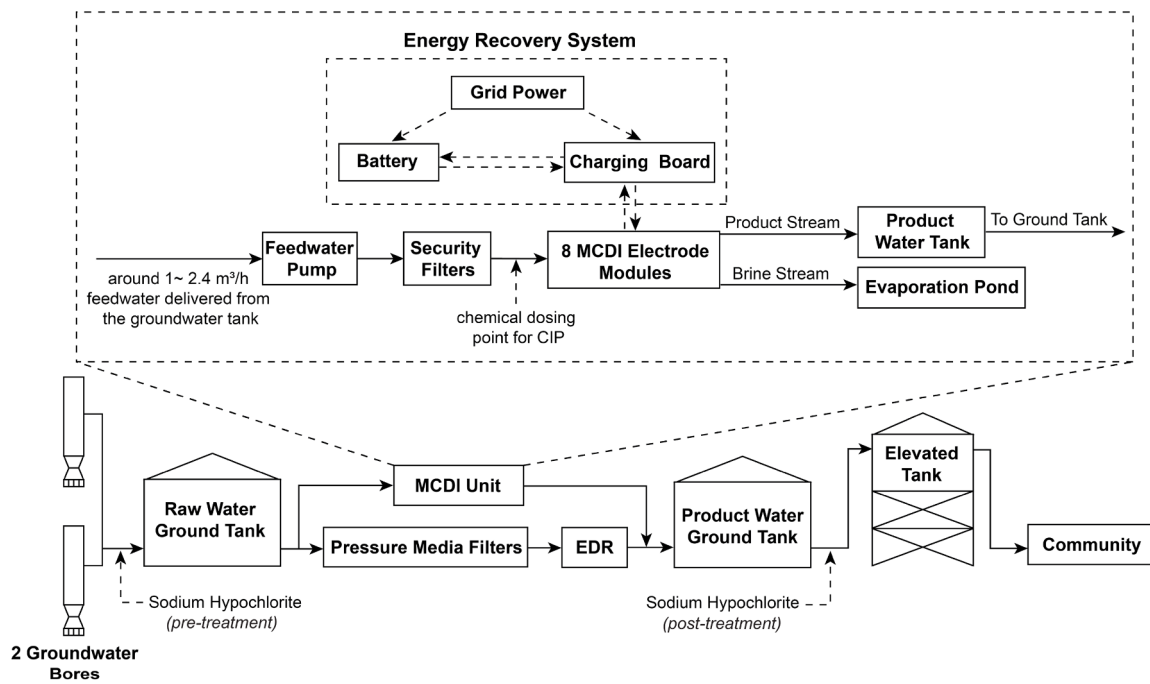


**Fig. 1.** Schematic diagram of the pilot-scale MCDI unit and the full-scale EDR unit of the groundwater treatment plant in the Northern Territory of Australia.

## 2.2. Operation and maintenance of the MCDI pilot unit

The MCDI electrode modules were operated in a cyclical manner in CC mode throughout the trial as CC operation can produce consistent quality of desalinated water and uses comparatively less energy than operation in CV mode (Kim et al., 2020). Fig. 2a illustrates a typical electrode (charging-discharging-idle) cycle of the two MCDI electrode operational strategies employed during the trial, namely constant current-reverse current discharge with the reversed current applied until the resulting voltage decreases to a positive cut-off voltage (termed CC-RCD-DPV) and constant current-reverse current discharge with the reversed current applied until the resulting voltage decreases to a negative cut-off voltage (termed CC-RCD-DNV). Note that we only controlled the applied direction and amplitude of the current based on the MCDI cell voltage in both CC-RCD-DPV and CC-RCD-DNV modes, which differs from the other commonly used constant voltage-reverse voltage discharge (CV-RVD) operational mode in which the voltage instead of the current is controlled to drive the electrode discharging. The distinctions between various MCDI operational modes are provided in SI Figure S2. Herein, one complete CC-RCD MCDI cycle comprises the following stages:

1. *Electrode charging and product discharge stage:* A CC of between 50 and 150 A is applied to polarize the carbon electrodes with rise in cell voltage (i.e., total potential differences between electrode pairs) associated with the buildup of electrical charge on the electrodes. Counter-ions of the opposite charge to the electrode or the functional groups of the IEM, i.e., cations for the cathode and the cation exchange membrane (CEM), and anions for the anode and the anion exchange membrane (AEM), migrate towards their respective electrodes and are stored in the EDL as shown in Fig. 2b. It is worth noting that as the CEM and AEM are slightly leaky to ions of the same charge as their functional groups, a relatively small number of co-ions will enter and possibly be retained in the electrode structure after several MCDI cycles (Zhao et al., 2012). Once the cell voltage reaches a cut-off value (typically <1.5 V to avoid the additional energy loss and electrode degradation caused by the Faradaic redox reactions that will occur at high voltages), the electrode charging

process will be terminated. Product water will continuously be generated after the initial period of electrode charging when the electrical conductivity (EC) has decreased to an acceptable value.

2. *Electrode discharging/regeneration and stopped flow stage:* Following the electrode charging stage, the applied constant current is reversed in order to discharge the electrode such that it is ready for the next charging-discharging-idle cycle. The electrode discharging/regeneration process is terminated when the cell voltage drops to a low positive value (i.e., 170 mV) in CC-RCD-DPV operation or to a pre-assigned negative voltage (i.e., -1000 mV) in CC-RCD-DNV operation. During positive (voltage) discharging as illustrated in Fig. 2c, the adsorbed counter-ions will be released from the electrode micropores and diffuse towards the flow channel. The electrode polarity remains the same as it is during the electrode charging step and may lead to insufficient ion desorption. As illustrated in Fig. 2d, when the cell voltage drops below 0 V during electrode discharging in CC-RCD, negative (voltage) discharging will commence and the polarity of the electrode pairs will be reversed, converting cations (or anions) remaining in the electrode region on the CEM (or AEM) side into counterions of the opposite electrode. The electrostatic attraction will promote ion desorption and ion migration towards the opposite electrode; however, it is difficult for the desorbed ions to penetrate the IEMs on the opposite side since these ions have the same charge as the functional groups of the opposite IEMs. As a result, electrode regeneration will be more effective. The process feedwater pump will not transport any water through the MCDI modules at this stage to minimize wastage of water in a process referred to as stopped flow.
3. *Electrode idle and brine discharge stage:* No current is applied at this stage and the process pump discharges the concentrated brine stream out of the electrode modules. Note that brine discharge will continue when the EC is still decreasing and has not reached steady state at the beginning of the electrode charging stage of the following cycle as indicated by white shading of the flow state in Fig. 2a.

Compared to the implementation of laboratory scale studies, it is unsafe in operation of large-scale systems to discharge the MCDI electrodes by short-circuiting since it results in generation of a large inrush

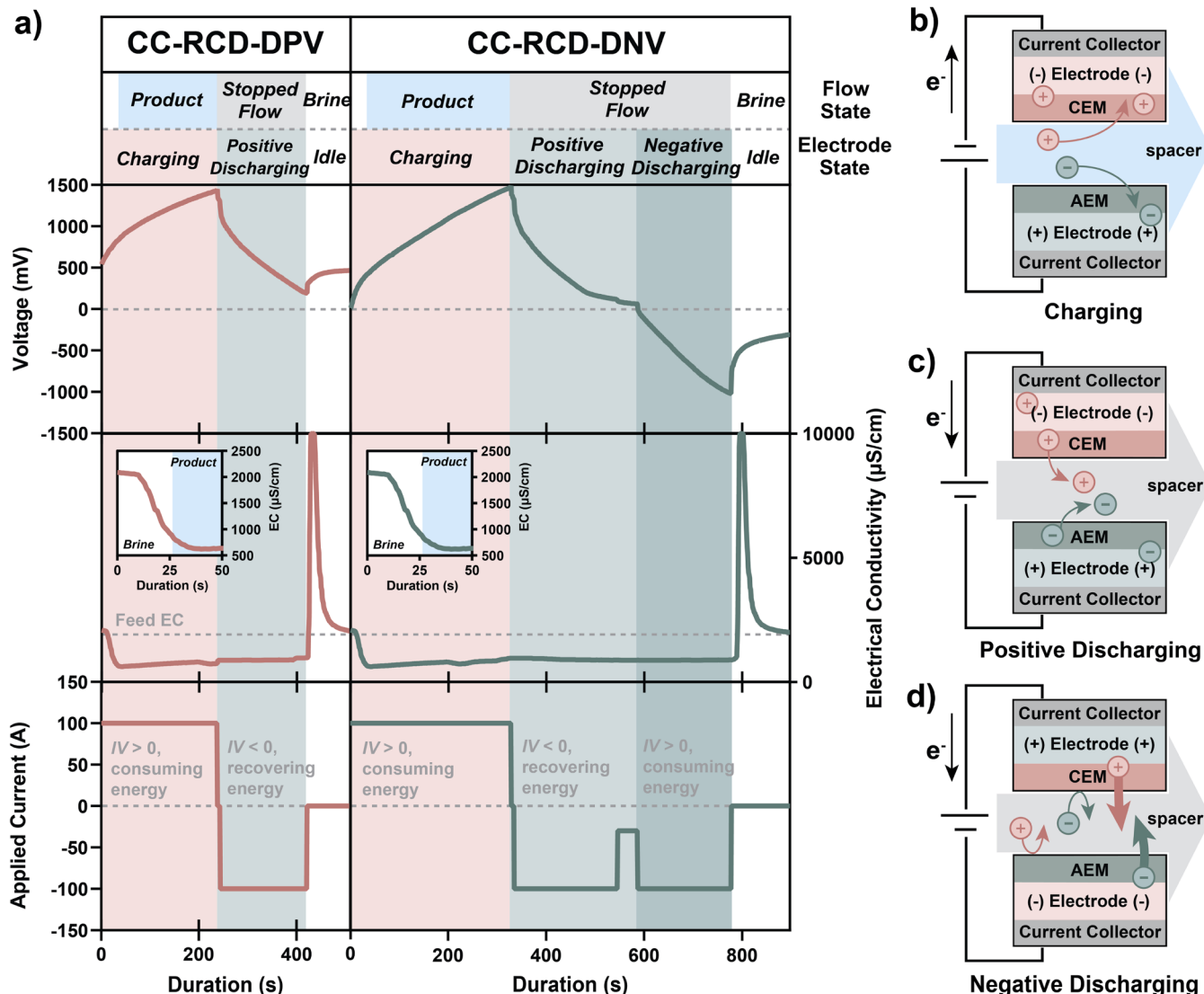


**Fig. 2.** Comparison of two operational modes in constant current operation showing a) variations in cell voltage, MCDI outlet electrical conductivity and applied current of a typical MCDI ion adsorption-desorption (or electrode charging-discharging-idle) cycle for CC-RCD-DPV and CC-RCD-DNV modes with different electrode and flow states highlighted in shading, and schematic views of b) ion adsorption during electrode charging, c) ion desorption during electrode positive (voltage) discharging, and d) ion desorption during electrode negative (voltage) discharging. CEM containing negatively charged functional groups, negatively charged electrode (cathode) and their counterions (cations) are shaded in red. AEM containing positively charged functional groups, positively charged electrode (anode) and their counterions (anions) are shaded in green.

current. If the cell voltage decreases to a value that is close to zero volt during the electrode positive discharging stage, it will pose difficulties in maintaining a high discharging current of  $>100$  A (Zhou et al., 2018). Therefore, controlled current electrode discharging to a relatively low (but non-zero) cut-off voltage was adopted during the positive discharging stage in this trial. Additionally, a passive discharging period at the end of the positive discharging stage was applied in CC-RCD-DNV operation to avoid the rapid increase in circuit temperature and possible associated electrical hazards as indicated by the negative current of different magnitude in Fig. 2a (the magnitude of this current is determined by the circuit resistance and is smaller than the normal discharging current). Due to the presence of series and parallel resistances in the circuit as demonstrated in SI Figure S3, a voltage jump is observed when the electrode charging and discharging stages are initiated. The voltage jump is larger when incomplete ion desorption occurs, which will shorten the duration of the electrode charging stage and affect MCDI performance metrics such as productivity and water recovery (He et al., 2023).

The unit was commissioned and operated from October 2021 to April 2023 as outlined in Table 1. The duration of the trial was 562 days with the unit operated for 1522.5 h in total. For unit maintenance, three clean-in-place (CIP) operations were performed using 30 litres of 5% hydrochloric acid to regenerate the electrode performance and remove any hardness-induced scale that may have formed in the hydraulic system of the unit over the long-term CC-RCD-DPV operation. After the last CIP, the MCDI operation was switched from the CC-RCD-DPV mode to the CC-RCD-DNV mode. Applied current and flowrate were varied as desired prior to each long-term operation in both CC-RCD-DPV and CC-RCD-DNV modes leading to changes in the duration of the MCDI adsorption-desorption cycles due to the different rates of salt removal. The changes in flow and electrode states within one MCDI adsorption-desorption cycle, as illustrated in Fig. 2a, were controlled automatically by the installed Siemens PLC.

**Table 1**

Summary of unit operation and maintenance information for different periods of the long-term MCDI trial.

Operational Mode	Period	Feed Flowrate (L/min/module)	Applied Current (A/module)	Total Operating Hours (h)	Number of Cycles
CC-RCD-DPV	1/10/2021 ~ 15/ 2/ 2022	4.2 ~ 6.4	90 ~ 125	370.5	8,979
	17/2/2022 ~ 24/ 5/ 2022	2.7 ~ 4.3	40 ~ 100	274.4	6,191
	26/5/2022 ~ 9/ 11/ 2022	2.7 ~ 4.8	50 ~ 85	214.0	4,086
	11/11/2022 ~ 14/ 4/ 2023	2.1 ~ 5.7	80 ~ 120	663.6	3,925
Over the Trial	562 days	2.1 ~ 6.4	40 ~ 125	1,522.5	23,181

### 2.3. Performance assessment

The desalination performance of each MCDI charging-discharging-idle cycle was evaluated using the indicators provided by Hawks et al. (2019b); i.e.

$$V_p = \int_{\Delta t_p} Q dt \quad (1)$$

$$V_b = \int_{\Delta t_b} Q dt \quad (2)$$

$$WR = \frac{V_p}{V_p + V_b} \quad (3)$$

where  $Q$  is the volumetric flowrate through one MCDI module,  $V_p$  is the product volume of the module,  $\Delta t_p$  is the duration of product discharge,  $V_b$  is the volume of the brine generated after the stopped flow stage,  $\Delta t_b$  is the duration of brine discharge, and WR is the water recovery.

The electrical conductivity reduction,  $\Delta EC$  ( $\mu\text{S}/\text{cm}$ ), was measured to assess the overall salt removal, which is given by:

$$\Delta EC = \frac{\int_{\Delta t_p} (\sigma_f - \sigma_p) dt}{\Delta t_p} \quad (4)$$

where  $\sigma_f$  is the feedwater EC, and  $\sigma_p$  is the product EC.

The productivity,  $P$  ( $\text{L}/\text{h}/\text{m}^2$ ), is given by:

$$P = \frac{V_p}{n \cdot A \cdot \Delta t_{cycle}} \quad (5)$$

where  $n$  is the number of cells (electrode pairs) in one stacked MCDI module,  $A$  is the projected facial area of the cell, and  $\Delta t_{cycle}$  is the total duration of one MCDI charging-discharging-idle cycle.

For the energy and economic assessment, we calculated the volumetric electrode energy consumption,  $E_v$  ( $\text{kWh}/\text{m}^3$ ), using the following

equations:

$$E_{in} = \sum_{i=1}^8 \int_{\Delta t_{cycle}} IV dt \text{ where } IV > 0 \quad (6)$$

$$E_{out} = \sum_{i=1}^8 \int_{\Delta t_{cycle}} IV dt \text{ where } IV < 0 \quad (7)$$

$$E_v = \frac{E_{in} - E_{out}}{V_p} \quad (8)$$

where  $I$  is the current applied,  $V$  is the cell voltage,  $E_{in}$  represents the total energy input to eight MCDI modules over one MCDI cycle,  $E_{out}$  represents the total energy that can be recovered from eight MCDI modules over one MCDI cycle. The current-voltage product,  $IV$ , is the power consumed (i.e.,  $IV > 0$ ) or recovered (i.e.,  $IV < 0$ ) for one MCDI module at a given time. Hence, the volumetric energy consumption of the entire MCDI system,  $E_v$  ( $\text{kWh}/\text{m}^3$ ), is given by:

$$E_t = E_v + E_{pump} + E_{valve} + E_{ancillary} \quad (9)$$

where  $E_{pump}$ ,  $E_{valve}$  and  $E_{ancillary}$  are the volumetric energy consumption of pumps, valves and ancillary electrical systems, respectively. It is assumed that apart from passive discharging, all the energy during the electrode positive discharging can be recovered with resistive losses ignored in the calculation.

In the comparative assessment of economic efficiency of different water treatment systems, the capital recovery factor,  $CRF$ , the equivalent annual cost for the investment of a specific piece of equipment,  $EAC_{equipment}$  (AU\$/year), and the equivalent annual capital cost,  $C_{capital}$  (AU\$/year), were evaluated using the equations provided by Lamei et al. (2008) and Papavinasam (2014):

$$CRF = \frac{i_r \cdot (i_r + 1)^t}{(i_r + 1)^t - 1} \quad (10)$$

$$EAC_{equipment} = CRF \times C_{equipment} \quad (11)$$

$$C_{capital} = EAC_{major} + EAC_{others} \quad (12)$$

where  $i_r$  is the rate charged on the loan for the capital cost or the discount rate (8 % was used in this study),  $t$  is the expected lifetime of a piece of equipment,  $C_{equipment}$  is the capital cost of a piece of equipment,  $EAC_{major}$  is the equivalent annual capital cost of major components, and  $EAC_{others}$  is the equivalent annual capital cost of other components. The classification of major and other components of different water treatment systems and their respective unit price and lifetime are listed in SI Table S6.

The annual O&M costs of different systems,  $C_{O\&M}$  (AU\$/year), and the levelized cost of water,  $LCOW$  (AU\$/ $\text{m}^3$ ), were hence can be calculated by:

$$C_{O\&M} = C_{general O\&M} + C_{Labour \& Travel} \quad (13)$$

$$LCOW = \frac{C_{capital} + C_{O\&M}}{V_{p, annual}} \quad (14)$$

where  $C_{general O\&M}$  is the general O&M costs including the cost relating to energy consumption and chemical consumption of the water treatment system,  $C_{Labour \& Travel}$  is the cost of labour and relating travel for system services, and  $V_{p, annual}$  is the annual production of the water treatment system. Further information on assumptions used in the energy and economic assessment can be found in SI Section S5.

## 2.4. Water quality analyses

In this study, the feedwater EC and the MCDI product water EC were continuously monitored onsite using two digital conductivity sensors (CLS21D, Endress+Hauser). The concentrations of major inorganic ions, including  $\text{Ca}^{2+}$ ,  $\text{Mg}^{2+}$ ,  $\text{K}^+$ ,  $\text{Na}^+$ ,  $\text{SO}_4^{2-}$ ,  $\text{NO}_3^-$ ,  $\text{Cl}^-$  and  $\text{F}^-$ , and selected heavy metals were analysed from the monthly taken water samples by accredited laboratories offsite using various analysis methods such as inductively coupled plasma atomic emission spectrometry (ICP-AES), colorimetric flow analyser (CFA) and ion selective electrode (ISE) techniques (National Association of Testing Authorities, 2024). The composition of feed groundwater is listed in Table 2.

To assess the removal of major inorganic ions, ion concentration reduction,  $\langle \Delta c \rangle$  (mM) and removal efficiency,  $RE$  (%), were calculated by:

$$\langle \Delta c \rangle = \langle c_f \rangle - \langle c_p \rangle \quad (15)$$

$$RE = \frac{\langle \Delta c \rangle}{\langle c_f \rangle} \quad (16)$$

where  $\langle c_f \rangle$  is the ion concentration in the feedwater, and  $\langle c_p \rangle$  is the ion concentration in the product water.

The ion selectivity,  $\rho$ , was defined as:

$$\rho = \frac{RE_i}{RE_j} \quad (17)$$

where  $RE_i$  and  $RE_j$  are the  $RE$  of two competing ions (of the same polarity),  $i$  and  $j$ , respectively.

## 3. Results and discussion

### 3.1. MCDI performance over the trial

The overall unit performance for different operational modes is summarized in Table 3. Over the trial, the MCDI pilot unit has reduced the EC of the treated water from  $1710 \pm 90 \mu\text{S}/\text{cm}$  (equivalent to  $1025 \pm 50 \text{ mg/L TDS}$ ) to  $920 \pm 130 \mu\text{S}/\text{cm}$  (equivalent to  $550 \pm 80 \text{ mg/L TDS}$ ) with a water recovery of  $71.6 \pm 8.7 \%$ .

**Table 2**  
Chemical composition of the feed groundwater.

Parameter	Average and standard deviation values	ADWG value
TDS (mg/L) <sup>a</sup>	$1002.5 \pm 76.4$	< 600
EC ( $\mu\text{S}/\text{cm}$ ) <sup>a</sup>	$1684.6 \pm 101.4$	N/A
Hardness (mg $\text{CaCO}_3/\text{L}$ )	$245.4 \pm 14.2$	< 200
Alkalinity (mg $\text{CaCO}_3/\text{L}$ )	$382.9 \pm 17.8$	N/A
pH	$8.0 \pm 0.2$	$6.5 \sim 8.5$
$\text{Ca}^{2+}$ (mg/L)	$31.8 \pm 2.1$	N/A
$\text{Mg}^{2+}$ (mg/L)	$40.3 \pm 2.4$	N/A
$\text{K}^+$ (mg/L)	$54.5 \pm 2.9$	N/A
$\text{Na}^+$ (mg/L)	$252.3 \pm 26.9$	< 180
$\text{SO}_4^{2-}$ (mg/L)	$85.0 \pm 13.1$	< 250
$\text{CO}_3^{2-}$ (mg/L)	< 10	N/A
$\text{NO}_3^-$ (mg/L)	$84.6 \pm 11.6$	< 50
$\text{Cl}^-$ (mg/L)	$189.3 \pm 29.4$	< 250
$\text{F}^-$ (mg/L)	$2.4 \pm 0.2$	< 1.5
$\text{HCO}_3^-$ (mg/L)	$465.0 \pm 22.5$	N/A
$\text{SiO}_2$ (mg/L)	$59.5 \pm 3.7$	N/A
Fe (T) (mg/L)	< 0.02	< 0.3
Cu (T) (mg/L)	< 0.01	< 1
Uranium ( $\mu\text{g}/\text{L}$ )	$11.0 \pm 1.7$	< 20
Turbidity (NTU)	$0.7 \pm 0.7$	< 5
True Colour (HU)	< 2	< 15

<sup>a</sup> Note that the feed TDS and EC in this table differ slightly from those reported in later Section 3.1 and Section 3.4 because the data source for this table is water samples that were taken (~once every month) over the trial, while the feed and product TDS used in later sections are derived from inline sensors. Additionally, the data presented in this table were used in the simulation of brackish water reverse osmosis (BWRO) systems in Section 3.4 after charge balance.

TDS) with a water recovery of  $71.6 \pm 8.7 \%$ . Productivity of  $9.9 \pm 2.8 \text{ L/h/m}^2$  relevant to the projected facial area of the MCDI electrodes (equivalent to  $2.5 \pm 0.7 \text{ m}^3/\text{day/module}$ ) was achieved when the feed flowrate and the applied charging current ranged from  $2.1$  to  $6.4 \text{ L/min/module}$  and  $40$  to  $125 \text{ A/module}$ , respectively.

During the long-term CC-RCD-DPV operation from October 2021 to early August 2021, we observed performance deterioration with each successive cycle during continuous operation, especially in  $\Delta t_{cycle}$ , productivity and water recovery. This MCDI performance deterioration was confirmed, in complementary bench-scale studies, to be caused by incomplete electrode regeneration during the electrode discharging (He et al., 2023). These studies revealed that, due to the slow diffusion rate of divalent/multivalent ions, they are likely to be only partially desorbed if the electrode polarity is not reversed during the electrode discharging stage, thereby causing a large voltage jump and a shorter  $\Delta t_p$  for the following electrode charging (or ion adsorption) stage. This issue is likely to be exacerbated in stopped flow operation when the duration of the electrode discharging step is found to be even shorter than that in continuous flow operation (Biesheuvel et al., 2011; Tan et al., 2020). More problematically, insufficient ion desorption will also increase the chance of scale formation at the electrodes since slight leakage of co-ions through the membrane is unavoidable (Chen et al., 2018b; Zhao et al., 2012a). Possible approaches to facilitate the release of multivalent ions in CC-RCD-DPV operation are either through application of CIP procedures or intermittent operation of the unit as further discussed in Section 3.2. These two approaches, when applied to the unit operating in CC-RCD-DPV mode, resulted in a relatively short operating duration of  $6.0 \pm 5.1 \text{ h/day}$ . As illustrated in Fig. 3c, we decreased the applied charging current continuously from approximately  $125 \text{ A}$  to  $50 \text{ A}$  to ensure that  $\Delta t_p$  was long enough such that the product water quality could reach steady state and the product water quality could be maintained at an acceptable level without sacrificing too much productivity and water recovery (Fig. 3b). Even worse, the recovery of electrode performance was found to be less effective with time, especially after July 2022 when we observed an evident increasing trend in the product EC (Fig. 3a).

After operation in CC-RCD-DNV mode, it was immediately apparent that the performance of MCDI modules could be sufficiently regenerated during each electrode discharging cycle, which enabled the application of a higher charging current of  $80\text{--}120 \text{ A/module}$  compared with the  $50\text{--}85 \text{ A/module}$  charging current applied between the 2<sup>nd</sup> and the 3<sup>rd</sup> CIP (Fig. 3c). Both  $\Delta t_p$  and  $\Delta t_{cycle}$  experienced a sharp rise as outlined in Table 3, while the ratio of  $\Delta t_p$  to  $\Delta t_{cycle}$  increased slightly from  $37.9 \pm 5.0 \%$  to  $41.7 \pm 2.4 \%$ . As a result, a higher  $\Delta EC$  of  $870 \pm 130 \mu\text{S}/\text{cm}$  and a longer operating duration of  $13.9 \pm 8.0 \text{ h/day}$  could be achieved in CC-RCD-DNV mode compared with CC-RCD-DPV mode, while the productivity and the water recovery remained at  $9.4 \pm 2.2 \text{ L/h/m}^2$  and  $72.0 \pm 8.1 \%$ , respectively. It should be noted that we did not replace any of the electrode modules over the entire trial nor make any changes to the operating environment of the MCDI electrode modules before implementing the CC-RCD-DNV operation except application of another CIP with the same acid dosage as used in the previous two CIP procedures.

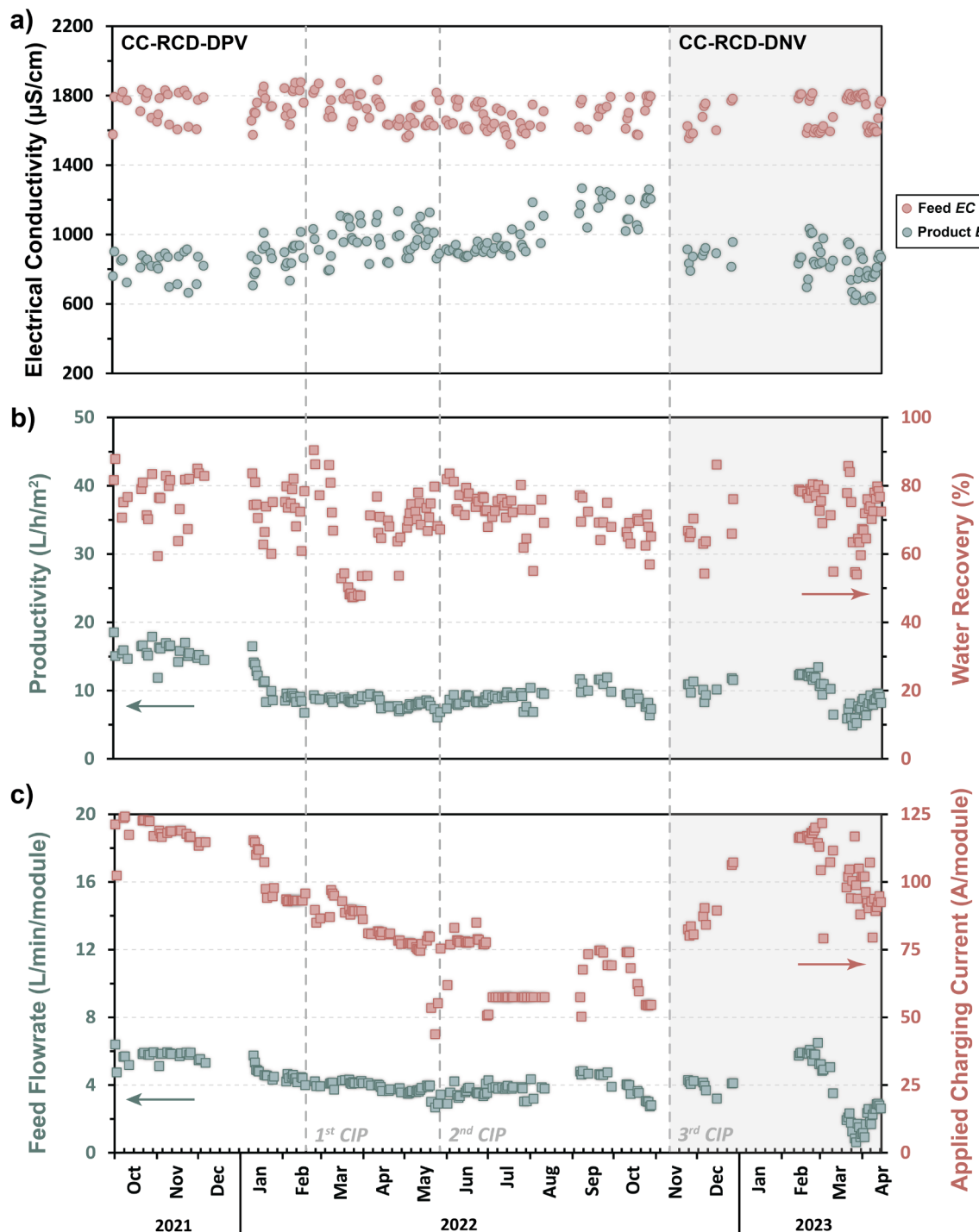
### 3.2. Impacts of CIP, intermittent operation and electrode discharging strategy on the performance of continuous CC-RCD operation

Fig. 4 depicts the declining trend of  $\Delta t_{cycle}$  and its impacts on productivity and water recovery in three selected cycles of the continuous CC-RCD-DPV operation. Compared with productivity and water recovery,  $\Delta EC$  was predominantly affected by feed flowrate and applied charging current instead of  $\Delta t_{cycle}$ , and did not show any obvious reduction in each cycle during one continuous operation.  $\Delta EC$  is thus not included as a performance indicator for discussion in this section. Decrease in  $\Delta t_{cycle}$  was observed from the first continuous CC-RCD-DPV operation with  $\Delta t_{cycle}$  decreasing from  $299$  to  $182 \text{ s}$  and  $\Delta t_p$  decreasing

**Table 3**

Summary of MCDI cycle time and overall performance under the CC-RCD-DPV and CC-RCD-DNV operation.

Operational Mode	$\Delta t_{cycle}$ (s)	$\Delta t_p$ (s)	Operating Duration (h/day)	$\Delta EC$ ( $\mu\text{S}/\text{cm}$ )	Productivity (L/h/m <sup>2</sup> )	Water Recovery (%)
CC-RCD-DPV	200 ± 85	80 ± 35	6.0 ± 5.1	760 ± 140	10.1 ± 2.9	71.4 ± 9.0
CC-RCD-DNV	690 ± 245	290 ± 105	13.9 ± 8.0	870 ± 130	9.4 ± 2.2	72.0 ± 8.1
Over the Trial	-	-	-	790 ± 140	9.9 ± 2.8	71.6 ± 8.7



**Fig. 3.** Average daily performance of the MCDI pilot unit over the trial: a) feed electrical conductivity (red dots) and product electrical conductivity (green dots), b) water recovery (red boxes) and productivity corresponding to the projected electrode module facial area (green boxes) when the unit was operating, and c) average applied charging current (red boxes) and feed flowrate (green boxes) of one MCDI module during the electrode charging stage. The time of implementation of CIP procedures are indicated by grey dashed lines and the period of CC-RCD-DNV operation is highlighted by grey shading.

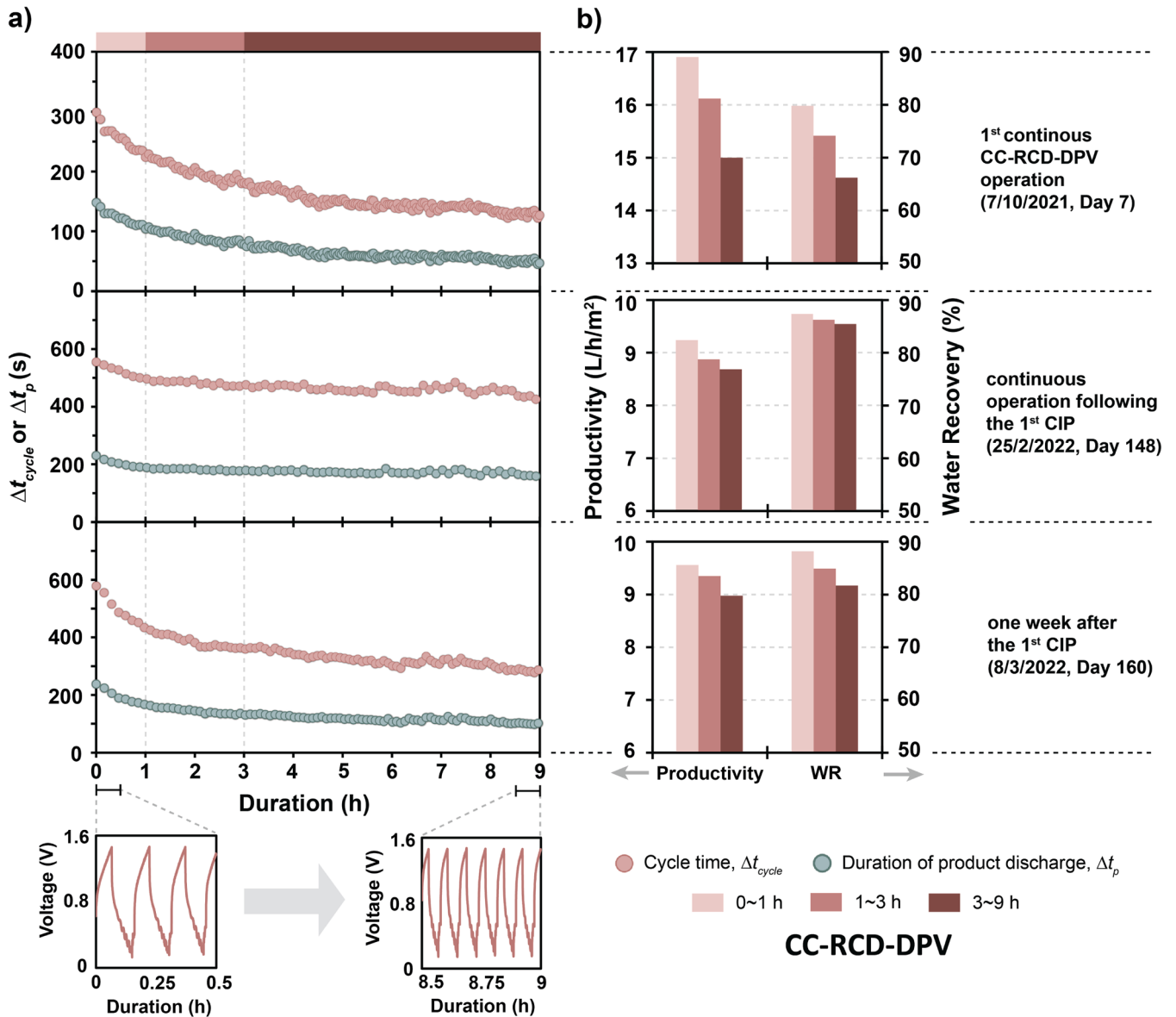


**Fig. 4.** Performance of three selected continuous CC-RCD-DPV operations: a) variations in cycle time ( $\Delta t_{cycle}$ ), duration of product discharge ( $\Delta t_p$ ), and cell voltage, and b) variations in average productivity and water recovery during different operation periods. Note that the feed flowrate and applied current remained constant throughout each continuous operation; however, a charging current of 123.6 A/module and a flowrate of 5.7 L/min/module was applied on Day 7, a charging current of 90.5 A/module and a flowrate of 4.0 L/min/module was applied on Day 148, and a charging current of 97.8 A/module and a flowrate of 4.1 L/min/module was applied on Day 160.

from 148 to 84 s within the first three hours of the operation.  $\Delta t_{cycle}$  and  $\Delta t_p$  further decreased by 56.2% (to 131 s) and 72.3% (to 41 s), respectively, over a span of nine hours. As a consequence, the average productivity decreased from 16.9 to 15.0 L/h/m<sup>2</sup> and the water recovery decreased from 79.8% to 66.2% for the nine-hour continuous operation.

CIP was found to be effective in inhibiting the rapid performance deterioration during continuous operation.  $\Delta t_{cycle}$  and  $\Delta t_p$  showed only a 22.0% decrease (from 545 to 425 s) and a 27.2% decrease (from 217 to 158 s) during the entire continuous operation that occurred following the CIP. However, only one week after the CIP, declines in  $\Delta t_{cycle}$  and  $\Delta t_p$  returned to 50.3% (from 578 to 287 s) and 57.1% (from 238 to 102 s) over a nine-hour continuous operation. Regarding other performance metrics, it is evident that CIP was more effective in maintaining productivity than water recovery. Productivity of the two continuous operations after the CIP on Day 148 and on Day 160 showed a similar reduction of 0.56 and 0.57 L/h/m<sup>2</sup> within nine hours, respectively.

However, a markedly faster decrease in  $\Delta t_{cycle}$  exacerbated its detrimental effect on water recovery. Water recovery for the first nine-hour continuous CC-RCD-DPV operation following the CIP consistently remained over 85%. Conversely, a more pronounced decline in water recovery was observed one week after the CIP, dropping from an average of 88.2% in the initial three hours of continuous operation to an average of 81.67% in the final six hours of continuous operation. This was because the ratio of  $\Delta t_p$  to  $\Delta t_{cycle}$  only decreased by 2.5% during operation on Day 148 but decreased by 5.7% during the operation on Day 160. It is worth noting that prior to the commencement of the two continuous operations after the CIP, the unit was idle (i.e., the unit operation was paused) for around nine hours to ensure the maximum regeneration of the electrode performance. The results suggest that CIP using 30 litres of 5% hydrochloric acid can successfully slow down the overall performance deterioration although its effect on stabilizing the MCDI performance will only last for a short period of time with more

frequent CIP subsequently required. The frequent need for CIP will greatly increase the maintenance cost, considering the unit is located at a remote location where the access to technicians is limited and shipping cost of chemicals is high. Moreover, frequent CIP may damage the IEMs and affect their ion separation performance (Chheang et al., 2022; Mei et al., 2018).

The other approach to restore electrode performance when the unit is operated in CC-RCD-DPV mode involves temporarily pausing the continuous operation. The effectiveness of this approach can be attributed to the presence of parallel resistance in the circuit, as demonstrated in SI Figure S3, which allows the self-discharging of MCDI electrodes to 0 volt with time when the electrodes are idle without the application of electric current to facilitate ion migration. As a result, the multivalent ions trapped within the carbon electrodes progressively diffuse to the spacer channel as the cell voltage decreases. Nevertheless, this intermittent operation approach was found to predominantly enhance performance of the first few MCDI cycles only following the restart of the unit with  $\Delta t_{cycle}$  subsequently dropping by nearly 50% over the course of each continuous operation as illustrated in SI Table S2. Therefore, we have trialled a range of different unit idle times ( $\Delta t_{down}$ , the time since the continuous operation was paused) to examine how variations in  $\Delta t_{down}$  influence the recovery of  $\Delta t_{cycle}$  and to explore if the timing of pausing and restarting the unit operation could be manipulated to make the most of the short period of high  $\Delta t_{cycle}$  and electrode performance. Whilst the result of the developed model was restricted to the exact operating conditions employed (i.e., applied charging current of 49.3 A/module and feed flowrate of 3.9 L/min/module), it still provided insights into the trade-offs between  $\Delta t_{down}$ ,  $\Delta t_{cycle}$  and MCDI electrode performance as demonstrated in SI Section S3. After validation using coefficient of determination ( $R^2$ ) as reported in SI Figures S6 and S7, the model was employed to predict the performance of unit operating in CC-RCD-DPV mode with consideration given to two different operation strategies: a one-off continuous operation after the pause (labelled “1 × 12 h” in Fig. 5a), and multiple pauses and operations of equal duration over 24 h (labelled “8 × 1.5 h” in Fig. 5b). The cumulative  $\Delta t_{cycle}$  and  $\Delta t_{down}$  were the same at 12 h per day for these two scenarios, but the model showed varied performance results. Although a single pause of 12 h resulted in a better recovery of  $\Delta t_{cycle,0}$  ( $\Delta t_{cycle}$  of the first cycle after the

restart of the unit operation), the rapid decline in  $\Delta t_{cycle}$  implied that most of that one-off operation was spent in the worst-performing region; if the unit was instead only paused for 1.5 h and then operated for 1.5 h, albeit with lower recovery in  $\Delta t_{cycle,0}$  compared with the former scenario, the unit was spending more time at higher  $\Delta t_{cycle}$  such that the overall performance in terms of productivity and water recovery was superior. Fig. 5c and d show that this strategy of multiple pauses and operations led to an increase in product volume of the MCDI unit by 0.56 m<sup>3</sup>/day and a reduction in brine volume of the MCDI unit by 0.76 m<sup>3</sup>/day, consequently elevating the water recovery by 6.2 % with fewer MCDI cycles over 24 h. Fewer cycles also resulted in reduced wear on solenoid valves and the processing pump. Although this operational strategy could result in a considerable improvement in overall unit performance without significant increase in the cost of maintenance of the unit, it does not address the underlying issue of performance deterioration stemming from the decline in  $\Delta t_{cycle}$ .

Operation in CC-RCD-DNV mode was trialled after 858.9 h of operation in CC-RCD-DPV following the third CIP. It can be clearly seen in Fig. 6a that both  $\Delta t_{cycle}$  and  $\Delta t_p$  could be maintained at over 700 s and 300 s, respectively, during the first continuous CC-RCD-DNV operation on Day 500. Although the total operating hours of the CC-RCD-DNV operation were longer than that of any CC-RCD-DPV operation period between two CIP procedures as outlined in Table 1,  $\Delta t_{cycle}$  and  $\Delta t_p$  remained stable at around 520 and 200 s during the final continuous CC-RCD-DNV operation on Day 562, respectively, when different feed flowrates and charging currents were applied. When comparing the MCDI performance metrics with time of one continuous operation, productivity was consistently over 12 L/h/m<sup>2</sup> with a difference between the maximum and the minimum productivity of 0.12 L/h/m<sup>2</sup> during the first continuous CC-RCD-DNV operation; similarly, in the final continuous operation, changes in productivity were minimal, with a difference between the maximum and the minimum productivity of 0.11 L/h/m<sup>2</sup>, which is considered within an acceptable margin of error instead of performance deterioration. A relatively constant water recovery of between 70% and 80% was also achieved for different feed flowrates and applied charging currents during these two operations as illustrated in Fig. 6b. Although there was no substantial increase in the productivity of each MCDI cycle in CC-RCD-DNV mode, the notable enhancement in

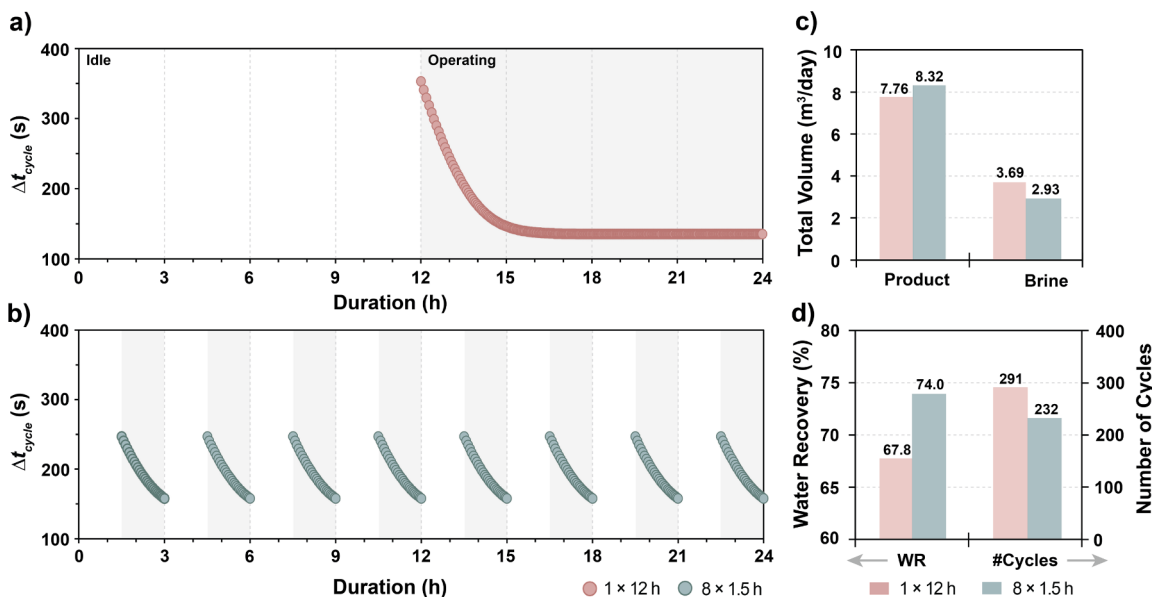


**Fig. 5.** Predicted cycle time when operating the unit for 12 h a day when the applied charging current of 49.3 A/module and feed flowrate of 3.9 L/min/module a) in a single run (labelled “1 × 12 h”) or b) in multiple runs of 1.5-hour duration (labelled “8 × 1.5 h”) with the grey shadings indicating periods of operation, and the relative performance of these two intermittent operational strategies in terms of c) total product and brine volume of the MCDI pilot unit and d) water recovery and number of cycles with red bars indicating the “1 × 12 h” strategy and green bars indicating the “8 × 1.5 h” strategy.

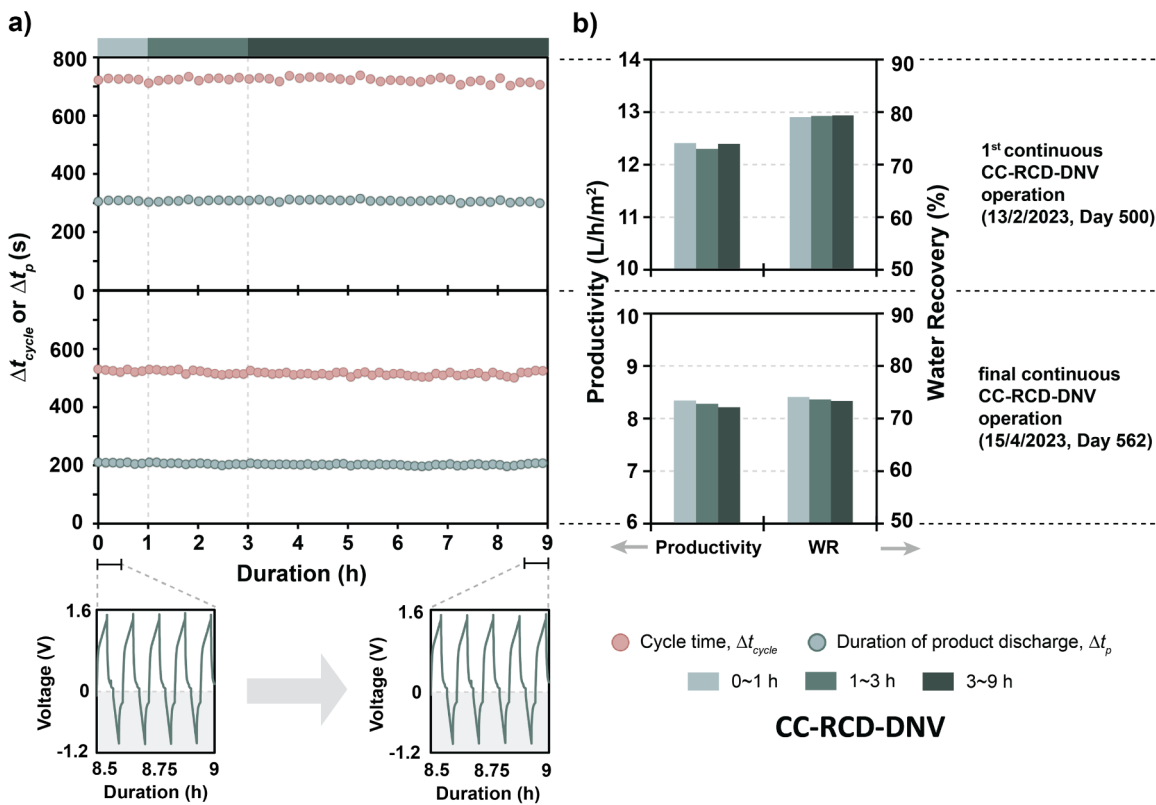


**Fig. 6.** Performance of three selected continuous CC-RCD-DNV operations: a) variations in cycle time ( $\Delta t_{cycle}$ ), duration of product discharge ( $\Delta t_p$ ), and cell voltage, and b) variations in average productivity and water recovery during different operation periods. Note that the feed flowrate and applied current remained constant throughout each continuous operation; however, a charging current of 116.9 A/module and a flowrate of 5.0 L/min/module was applied on Day 500, and a charging current of 90.1 A/module and a flowrate of 3.6 L/min/module was applied on Day 562.

operating duration (as shown in Table 3) and  $\Delta t_{cycle}$  stability (as shown in Fig. 6a) suggest that the total daily product volume would experience a significant increase as no additional pauses of continuous operation were needed to promote electrode regeneration.

Considering the reoccurrence of the rapid decline in  $\Delta t_{cycle}$  shortly after the CIP in CC-RCD-DPV operation, it can be inferred that the performance deterioration during the initial stage of a continuous operation is likely associated with the retention of dissolved ion species within the electrode pores rather than  $\text{CaSO}_4$  or  $\text{CaCO}_3$  scale formation. While we acknowledge that a gradual decrease in  $\Delta t_{cycle}$  and overall electrode performance might be inevitable due to possible scale formation in the long term (e.g., over a time span of several months) during continuous treatment, operation in CC-RCD-DNV mode greatly reduces the risk of ion build-up on the carbon electrode surfaces and enhances electrode performance regeneration. Furthermore, the frequency of implementation of CIP procedures can be significantly reduced for operation in CC-RCD-DNV mode, with no need for additional temporary pauses in unit operation to recover system performance.

### 3.3. Removal of major inorganic ions

Comparative removal of major ionic species in real groundwater was investigated during this long-term MCDI trial. In general, small-mdivalent ions are more favoured and have higher RE than large-monovalent ions in MCDI if their molar concentration are the same with this behaviour attributed to their differences in electrostatic attraction and abilities to screen the surface charge of the electrodes (Gamaethiralalage et al., 2021; Kim et al., 2019; Mossad and Zou, 2012; Seo et al., 2010; van Limp and van der Wal, 2014; Wang and Lin, 2019; Xu et al., 2008). Herein, we examine  $\langle \Delta c \rangle$  and RE of major inorganic ions over the course of the field trial for different MCDI operational modes.

For both CC-RCD-DPV and CC-RCD-DNV operations, the feedwater and the product TDS concentration remained at approximately 1000 mg/L and 470 mg/L, respectively. Variations in the concentration of inorganic ions with time are illustrated in Figure S4 of the SI.

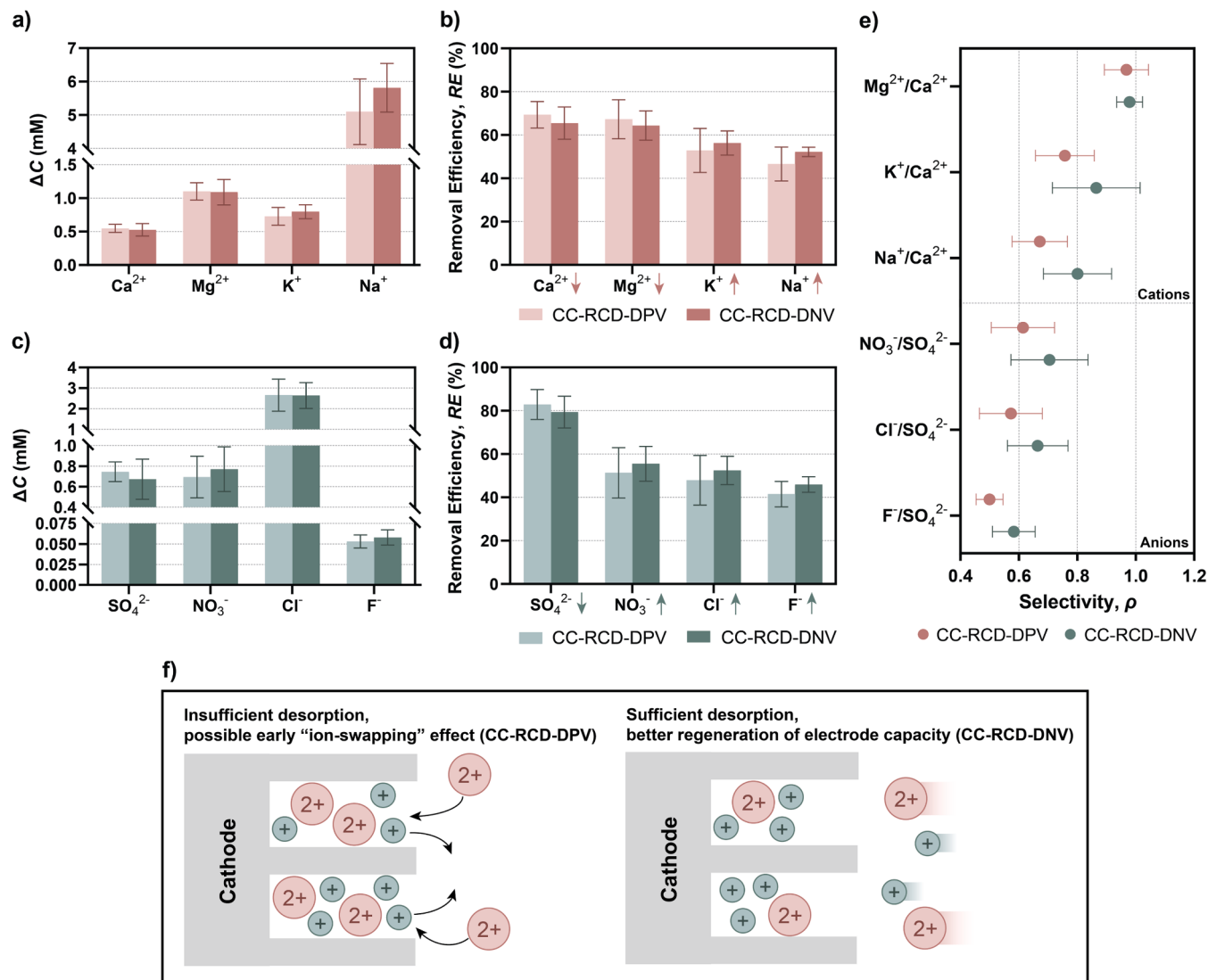
The ion composition of the feedwater and preferential removal of different monovalent and divalent ions over the entire trial are provided in Table 4. For mixed salt feed streams, RE is strongly related to two ion properties: i) ionic charge and ii) hydrated ionic size. The RE for cations was in the order of  $\text{Ca}^{2+} > \text{Mg}^{2+} > \text{K}^+ > \text{Na}^+$  with an average  $\rho$  of 0.97, 0.78 and 0.70 for  $\text{Mg}^{2+}/\text{Ca}^{2+}$ ,  $\text{K}^+/\text{Ca}^{2+}$  and  $\text{Na}^+/\text{Ca}^{2+}$  respectively as shown in Table 4. When comparing cations with the same charge, such as  $\text{Ca}^{2+}$  and  $\text{Mg}^{2+}$  (or  $\text{K}^+$  and  $\text{Na}^+$ ), their RE is primarily determined by the hydrated ionic size. Hence, it is expected that removal of  $\text{Ca}^{2+}$  and  $\text{K}^+$  will be more preferred, respectively, than  $\text{Mg}^{2+}$  and  $\text{Na}^+$ , due to their smaller hydrated radii and hydration ratio. For the anion RE,  $\text{SO}_4^{2-} > \text{NO}_3^- > \text{Cl}^- > \text{F}^-$  with an average  $\rho$  of 0.64, 0.60 and 0.52 for  $\text{NO}_3^-/\text{SO}_4^{2-}$ ,  $\text{Cl}^-/\text{SO}_4^{2-}$  and  $\text{F}^-/\text{SO}_4^{2-}$  respectively. The significant difference in the RE of  $\text{SO}_4^{2-}$  compared to that of monovalent anions can be explained by the difference in ionic charge. In contrast to the results of this study,  $\text{SO}_4^{2-}$  was less preferred than monovalent ions in the work by Hassanvand et al. (2018). This could potentially be caused by the narrow pore size distribution (micropore radius ranging from 3.5 to 3.75 Å) of their carbon electrodes, which was comparable to the hydrated radius of  $\text{SO}_4^{2-}$  (3.79 Å), making  $\text{SO}_4^{2-}$  more prone to ion sieving effects. Hence, in addition to ion properties, the properties of the MCDI electrode and, potentially, the ion exchange membranes can also influence the ion selectivity. Several previous studies have already been conducted, demonstrating the important role of carbon pore structure in ion selectivity (Cerón et al., 2020; Hawks et al., 2019a).

Changes in  $\langle \Delta c \rangle$  of different inorganic ions are influenced by both the  $\langle c_f \rangle$  and RE of these ions. Despite exhibiting the lowest RE of the various

**Table 4**

Properties of major inorganic ions (from Nightingale, 1959 and Vanysek, 1993) and removal performance over the trial.

Parameter	Unit	Cations				Anions			
		Ca <sup>2+</sup>	Mg <sup>2+</sup>	K <sup>+</sup>	Na <sup>+</sup>	SO <sub>4</sub> <sup>2-</sup>	NO <sub>3</sub> <sup>-</sup>	Cl <sup>-</sup>	F <sup>-</sup>
Properties <sup>a</sup>	Ionic Charge	-	2	2	1	1	2	1	1
	Hydrated Radius	Å	4.12	4.28	3.31	3.58	3.79	3.35	3.32
	Ionic Radius	Å	0.99	0.65	1.33	0.95	2.90	2.64	1.81
	Hydration Ratio	-	4.16	6.58	2.49	3.77	1.31	1.27	1.83
	Diffusion Coefficient ( $\times 10^{-9}$ )	$\text{m}^2/\text{s}$	0.79	0.706	1.96	1.33	1.07	1.90	2.03
Ion Removal over the Trial <sup>b</sup>	$\langle \Delta c \rangle$	mM	0.79 ± 0.05	1.66 ± 0.10	1.39 ± 0.07	10.92 ± 1.17	0.88 ± 0.14	1.35 ± 0.18	5.32 ± 0.83
	Removal Efficiency, RE	%	68.47 ± 6.34	66.57 ± 8.38	53.73 ± 9.16	48.00 ± 7.24	82.00 ± 6.98	52.38 ± 10.72	49.05 ± 10.45
Ion Selectivity, $\rho$ <sup>b</sup>	-	-	0.97 ± 0.07	0.78 ± 0.12	0.70 ± 0.11	-	0.64 ± 0.12	0.60 ± 0.11	0.52 ± 0.06

<sup>a</sup> Ion concentration, removal efficiency, and ion selectivity are reported in the format of mean ± standard deviation.<sup>b</sup> Ion selectivity reported in this table is calculated by dividing the removal efficiency of the cation or the anion of interest by the removal efficiency of Ca<sup>2+</sup> or SO<sub>4</sub><sup>2-</sup>.

**Fig. 7.** Removal of major inorganic ions during long-term CC-RCD-DPV and CC-RCD-DNV operations: average concentration reduction of a) cations and c) anions, average removal efficiency of b) cations and d) anions with arrows indicating the variations after the implementation of CC-RCD-DNV operation, e) selectivity of competing cations over Ca<sup>2+</sup> and competing anions over SO<sub>4</sub><sup>2-</sup>, and f) illustration of ion adsorption when the desorption of divalent ions is either “insufficient” or “sufficient” in the previous cycle (as is the case in CC-RCD-DPV mode compared to CC-RCD-DNV mode).

cations,  $\text{Na}^+$  was the most adsorbed cation with a  $\langle \Delta c \rangle$  of  $5.28 \pm 0.96$  mM as the  $\langle c_f \rangle$  of  $\text{Na}^+$  was much higher than that of other ions. The  $\langle \Delta c \rangle$  of other cations decreased in the order  $\text{Mg}^{2+} > \text{K}^+ > \text{Ca}^{2+}$ , reducing from  $1.10 \pm 0.14$  mM to  $0.54 \pm 0.07$  mM, which is consistent with their order in  $\langle c_f \rangle$ . Similarly,  $\text{Cl}^-$  was the most adsorbed anion with a  $\langle \Delta c \rangle$  of  $2.26 \pm 0.72$  mM due to its higher  $\langle c_f \rangle$  compared with that of other anions. Although the  $\langle c_f \rangle$  of  $\text{NO}_3^-$  was higher than that of  $\text{SO}_4^{2-}$ , more  $\text{SO}_4^{2-}$  was adsorbed than  $\text{NO}_3^-$  with a  $\langle \Delta c \rangle$  of  $0.73 \pm 0.12$  mM with this behaviour attributed to the significantly higher *RE* of  $\text{SO}_4^{2-}$ .

We explored the impact of different electrode discharging strategies on the selective removal of ions. Although the *RE* amongst different competing ions in CC-RCD-DPV and CC-RCD-DNV modes followed the same order of  $\text{Ca}^{2+} > \text{Mg}^{2+} > \text{K}^+ > \text{Na}^+$  for the cations and  $\text{SO}_4^{2-} > \text{NO}_3^- > \text{Cl}^- > \text{F}^-$  for the anions, an obvious increase in *RE* of monovalent ions and a decrease in *RE* of divalent ions can be seen in Fig. 7b and d. The average *REs* of  $\text{Ca}^{2+}$  and  $\text{Mg}^{2+}$  were reduced by 3.85% and 2.88%, whereas the average *REs* of  $\text{K}^+$  and  $\text{Na}^+$  were enhanced by 3.41% and 5.56%, respectively, in CC-RCD-DNV compared with CC-RCD-DPV. As for the anions, a decrease of 3.53% in the average *RE* of  $\text{SO}_4^{2-}$  was observed in CC-RCD-DNV compared with CC-RCD-DPV while the average *RE* of  $\text{NO}_3^-$ ,  $\text{Cl}^-$  and  $\text{F}^-$  increased by 4.17%, 4.50%, and 4.43%, respectively. Hence, a higher extent of monovalent ion removal was achieved by implementing negative discharging in CC-RCD-DNV. As illustrated in Fig. 7a and c,  $\langle \Delta c \rangle$  of  $\text{K}^+$ ,  $\text{Na}^+$ ,  $\text{NO}_3^-$  and  $\text{F}^-$  increased by 0.07, 0.72, 0.08, 0.005 mM, respectively, on changing from positive to negative voltage discharging while the extent of  $\text{Cl}^-$  removal remained almost unchanged. Varying levels of decrease in ion removal on changing from positive to negative voltage discharging were observed for divalent ions with the extent of change in  $\text{Ca}^{2+}$ ,  $\text{Mg}^{2+}$ , and  $\text{SO}_4^{2-}$  removal ranging from 0.01 mM to 0.07 mM. As illustrated in Fig. 7e, a small increase ( $\sim 0.01$ ) in the  $\rho$  of  $\text{Mg}^{2+}/\text{Ca}^{2+}$  was observed after the implementation of CC-RCD-DNV mode with this similarity attributed to the same ionic charge of these cations. Compared with CC-RCD-DPV, although the *RE* of divalent ions was still higher than that of monovalent ions in CC-RCD-DNV mode, the  $\rho$  of monovalent cations over  $\text{Ca}^{2+}$  increased by 0.11 for  $\text{K}^+$  and 0.13 for  $\text{Na}^+$ . Similarly, the  $\rho$  of monovalent anions, including  $\text{NO}_3^-$ ,  $\text{Cl}^-$ , and  $\text{F}^-$  over  $\text{SO}_4^{2-}$ , increased by  $0.08 \sim 0.09$ . This enhanced monovalent ion selectivity over divalent ion selectivity in CC-RCD-DNV operations aligned with our expectation that divalent ions would be desorbed more effectively and retained less within the electrodes. The differences in ion selectivity between CC-RCD-DPV and CC-RCD-DNV operations might also be explained by an “ion-swapping” effect. Hou and Huang (2013), Zhao et al. (2012b), and Hassanvand et al. (2018) reported that divalent ions (typically  $\text{Ca}^{2+}$ ) gradually replace the adsorbed monovalent cations in a mixed ion solution over time due to the stronger interaction between divalent ions and the electrode surface. As indicated in Fig. 7f, if the divalent ions remain within the electrode pores instead of being completely desorbed during the electrode discharging (or ion desorption) stage during continuous CC-RCD-DPV operation, the “ion-swapping” effect might be more significant than is the case for CC-RCD-DNV operation, thereby contributing to a decrease in the *RE* of divalent ions. It can be also inferred by the ion selectivity results that the accumulation of divalent ions most likely occurred at the electrode pores instead of at the IEMs and the spacer channel during CC-RCD-DPV operation. Negative discharging in CC-RCD-DNV reverses the electrode polarity, resulting in a stronger electrostatic attraction experienced by the ions remaining at the electrode region, which helps prevent the early occurrence of the possible “ion-swapping” effect and resolves the issue of insufficient ion desorption, particularly for divalent ions, during the positive discharging stage of CC-RCD operation.

### 3.4. Energy and economic efficiency for brackish groundwater desalination in remote locations: MCDI versus BWRO and EDR

This section presents the comparative analysis results of energy consumption and LCOW of different water treatment technologies, including MCDI, simulated BWRO and EDR, in treating groundwater for the purpose of potable water supply in remote locations. Based on the feedwater composition, the required daily capacity, the final product TDS and the achievable maximum water recovery without the risk of significant membrane fouling, two BWRO systems of different capacities (as provided in SI Section S4) were simulated by using Dupont’s Water Application Value Engine (WAVE™) design software. Acid dosing for pH adjustment and antiscalant dosing were included in the pre-treatment step of the system. In the post-treatment step, blending the feed brackish groundwater with the BWRO permeates was considered for water remineralization as adopted in other studies (Al-Obaidi et al., 2023; Duranceau, 2009; Pearson et al., 2021). Additionally, bleach dosing was considered after the blending step for water disinfection.

The average energy consumption to reduce the feed TDS from over 1000 mg/L to 500 mg/L using the pilot-scale MCDI unit (of a capacity of 20 m<sup>3</sup>/day) was 0.55 kWh/m<sup>3</sup> for operation in CC-RCD-DPV mode and 0.66 kWh/m<sup>3</sup> for operation in CC-RCD-DNV mode. The additional energy consumption in CC-RCD-DNV mode is attributed to the increase in electrode energy consumption during the negative discharging stage. In contrast, the simulated BWRO system with a similar daily production capacity and a water recovery of 60% required significantly higher energy consumption of around 2.37 kWh/m<sup>3</sup> to achieve a similar extent of TDS reduction. This finding is consistent with the conclusion drawn from studies by Zhao et al. (2013) that the energy consumption of the RO system is expected to be more than double that of the MCDI system when reducing the feed TDS from approximately 1000 to 500 mg/L. This is because the energy is used to drive the movement of ions in MCDI instead of water as is the case in BWRO, rendering BWRO less energy efficient in desalinating water with a salinity of below 2000 mg/L TDS. Moreover, a portion of the energy used in removing ions from solution during the charging stage in MCDI operation is stored in the electrodes and can be recovered during the positive voltage discharging stage (Dlugolecki and van der Wal, 2013; Tan et al., 2020). However, considering the additional life cycle cost and the relatively small residual energy that can be regained from the small volume of brine, energy recovery systems are not universally installed in BWRO systems, especially in small-scale systems like the ones simulated in this study (Pan et al., 2020; Xu et al., 2022).

By scaling up the MCDI system to a capacity of 1000 m<sup>3</sup>/day (similar to the capacity of the parallel EDR unit), the energy consumption of processing pumps and ancillary components were expected to reduce by around 0.07 kWh/m<sup>3</sup> and more than 0.05 kWh/m<sup>3</sup> in both CC-RCD-DPV and CC-RCD-DNV modes, thereby leading to a total energy consumption of 0.40 kWh/m<sup>3</sup> in CC-RCD-DPV mode and 0.53 kWh/m<sup>3</sup> in CC-RCD-DNV mode. The total energy consumption of the simulated 1000 m<sup>3</sup>/day BWRO system was also expected to decrease to 0.83 kWh/m<sup>3</sup>. Overall, the total system energy consumption of various water treatment systems with a capacity of 1000 m<sup>3</sup>/day follows the order of MCDI (CC-RCD-DPV) (0.40 kWh/m<sup>3</sup>) < MCDI (CC-RCD-DNV) (0.53 kWh/m<sup>3</sup>) < EDR (0.67 kWh/m<sup>3</sup>) < BWRO (0.83 kWh/m<sup>3</sup>) with further information provided in SI Table S7.

**Table 5** and **Table 6** summarize the economic assessment results of the water treatment systems of interest for two different daily production capacities. The field trial has demonstrated that the MCDI both operating in CC-RCD-DPV and CC-RCD-DNV modes required lower maintenance demands, especially in chemical consumption, than EDR and the simulated BWRO systems. Based on our simulation results, it appears that  $C_{\text{general O\&M}}$  (the O&M costs relating to energy and chemical consumptions) of the MCDI unit was approximately 1/10 of that of the BWRO systems for both 20 m<sup>3</sup>/day and 1000 m<sup>3</sup>/day systems, and approximately half of that of the 1000 m<sup>3</sup>/day EDR system. This

**Table 5**Summary of economic assessment on 20 m<sup>3</sup>/day MCDI and BWRO systems.

		MCDI (Trial Unit)		Simulated BWRO System 1
		CC- RCD- DPV	CC- RCD- DNV	
	Production (m <sup>3</sup> /day)		20	
	Feed TDS (mg/L)		1025.1 ± 52.9	
	Product TDS (mg/L)	571.0	498.1	500
		± 76.9	± 60.6	
	Water Recovery (%)	60 ~ 90	60 ~ 90	60
Capital Costs, <i>C<sub>capital</sub></i>	Major Components (AU\$/year) <sup>a</sup>	5,009	5,009	2,551
O&M Costs, <i>C<sub>O&amp;M</sub></i>	Other Components (AU\$/year) <sup>a</sup>	684	684	432
	<b>Subtotal (AU\$/year)</b>	<b>5,693</b>	<b>5,693</b>	<b>2,983</b>
General O&M <sup>b</sup>	Energy Cost (AU \$/year) <sup>c</sup>	1,634	1,961	7,042
	Acid Cost (AU \$/year) <sup>d</sup>	698	96	11,006
	Bleach Cost (AU \$/year)	45	45	45
	Antiscalant Cost (AU\$/year)	–	–	251
	Water Cost for Pure Water	–	–	780
	Cleaning (AU \$/year)			
	<i>C<sub>general O&amp;M</sub></i> (AU \$/year)	<b>2,377</b>	<b>2,101</b>	<b>19,123</b>
Labour and Travel <sup>b</sup>	Essential Services Operator (AU \$/year)	2,756	2,756	2,756
	Technicians (AU \$/year)	34,344	17,172	68,688
	Travel and Chemical Transportation (AU\$/year)	7,200	3,600	14,400
	<i>C<sub>Labour &amp; Travel</sub></i> (AU \$/year)	<b>44,300</b>	<b>23,528</b>	<b>85,844</b>
	<b>Subtotal (AU\$/year)</b>	<b>46,677</b>	<b>25,629</b>	<b>104,967</b>
<i>C<sub>capital</sub> + C<sub>O&amp;M</sub></i> (AU\$/year)		<b>52,370</b>	<b>31,322</b>	<b>107,949</b>
LCOW (AU\$/m <sup>3</sup> )		<b>7.174</b>	<b>4.291</b>	<b>14.788</b>

<sup>a</sup> Major components include RO elements and RO pressure vessels, MCDI modules and EDR stacks. Other components include process pumps, chemical dosing pumps and MCDI batteries. Further information is provided in SI Section S5a.

<sup>b</sup> Cost evaluation on general O&M and labour and travel was based on the information outlined in Section S5 of the SI.

<sup>c</sup> Energy consumption of specific components of MCDI systems in two operational modes and the simulated BWRO system can be found in Table S4 of the SI.

<sup>d</sup> Acid consumption of the MCDI system is the actual consumption observed over the trial, whereas the acid consumption of the simulated BWRO system is calculated based on WAVE™'s simulation results.

significant differences in *C<sub>general O&M</sub>* between the BWRO and MCDI systems are prominently caused by the substantial consumption of hydrochloric acid for pH adjustment at the pre-treatment step of the BWRO systems, which is commonly employed to prevent scale formation. MCDI also showed outstandingly low *C<sub>Labour & Travel</sub>* (the cost of labour and relating travel for system maintenance) compared with the simulated BWRO and EDR systems as less frequent CIP is required. Note that the assumptions used in SI Table S8 to estimate *C<sub>Labour & Travel</sub>* are of particular relevance in this specific trial location. Additionally, MCDI electrode charging and discharging are fixed within a range of low DC voltages, making it amenable to operation using photovoltaic energy in remote areas with no grid connection, which might further reduce the O&M costs of MCDI systems (Bales et al., 2023; Tan et al., 2018).

Although MCDI systems require a higher *C<sub>capital</sub>* attributed to the remarkable differences in unit prices of major components, i.e., MCDI modules, BWRO elements and pressure vessels, and EDR stacks, the

LCOW of the MCDI was still estimated to be lower than BWRO and EDR systems for this brackish groundwater desalination application in remote locations. It was found that the LCOW of the MCDI pilot unit dropped from AU\$7.174/m<sup>3</sup> to AU\$4.291/m<sup>3</sup> by implementing the CC-RCD-DNV mode. In contrast, the LCOW of the simulated BWRO system 1 with a capacity of 20 m<sup>3</sup>/day was projected to be AU\$14.788/m<sup>3</sup>. The LCOW of different water treatment systems with a capacity of 1000 m<sup>3</sup>/day follows the order of MCDI (CC-RCD-DNV) (AU\$1.059/m<sup>3</sup>) < MCDI (CC-RCD-DPV) (AU\$1.146/m<sup>3</sup>) < EDR (AU\$1.335/m<sup>3</sup>) < BWRO (AU\$2.307/m<sup>3</sup>).

### 3.5. Implications for future scaled-up MCDI applications: water-energy trade-offs

As discussed, the insufficient desorption of ions in CC operation has been effectively addressed by discharging the electrodes to a negative cell cut-off voltage. Although operation in CC-RCD-DNV mode stabilizes the performance and minimizes the scaling risk compared to alternate MCDI operational modes, it will result in an increase in system energy consumption by more than 0.10 kWh/m<sup>3</sup> if the electrodes are discharged to -1 volt in every MCDI cycle, as suggested by our trial results. The MCDI pilot unit described here was powered by the grid as water productivity and water recovery were of higher priority than energy efficiency in this field trial. However, the increase in energy consumption resulting from application of negative voltage discharging could potentially pose a challenge for MCDI use in off-grid locations. Additionally, given that the proportion of divalent ions to monovalent ions in feedwaters is likely to vary depending on the particular location and/or water treatment application, performance deterioration arising from insufficient desorption of divalent ions could be less severe in some instances. Alternating CC-RCD-DNV operation and CC-RCD-DPV operation or other O&M approaches would consequently be more preferred in particular scenarios. As envisaged in Section S6 of the SI, the following trade-offs amongst different MCDI performance metrics would be of interest to investigate in future work, and can be leveraged based on different MCDI applications to foster the upscaling of the MCDI technology: a) trade-offs amongst energy efficiency, water efficiency and product quality ascribed to changes in operating parameters such as feed flowrate and applied current, b) a trade-off between energy efficiency and water efficiency attributed to different MCDI operational modes, and c) a trade-off between maintenance costs and operating costs resulting from varying frequencies of CIP and electrode discharging strategies.

## 4. Conclusions

A long-term MCDI trial study was conducted at a small community in the Northern Territory of Australia in order to explore the feasibility of applying this technology to production of potable water meeting Australian Drinking Water Guidelines from groundwaters with high TDS concentration in remote locations. It has been demonstrated that the 8-electrode MCDI system can consistently reduce the salt concentration to the required palatable level of around 550 ± 80 mg/L TDS with a relatively high water recovery of 71.6 ± 8.7 %. However, rapid performance deterioration caused by the insufficient desorption of multivalent ions during the electrode discharging stage was observed during the continuous CC-RCD-DPV operation.

We found that both CIP and a modified operating procedure involving temporarily pausing the continuous operation could alleviate the performance deterioration during the CC-RCD-DPV operation; however, these procedures could not fundamentally counteract the detrimental effect of declines in  $\Delta t_{cycle}$  on MCDI cycle performance. To address this issue, operation in CC-RCD-DNV mode in which the electrode discharging was terminated at a negative cell cut-off voltage was adopted to enhance the stability of long-term MCDI operation. Although the productivity and water recovery of the MCDI cycle during the CC-

**Table 6**Summary of economic assessment on 1000 m<sup>3</sup>/day MCDI, BWRO and EDR systems.

	General O&M <sup>b</sup>	MCDI (Scaled-up System)		Simulated BWRO system 2	EDR
		CC-RCD-DPV	CC-RCD-DNV		
		Production (m <sup>3</sup> /day)		1000	
Capital Costs, $C_{\text{capital}}$		Feed TDS (mg/L)		1025.1 ± 52.9	
		Product TDS (mg/L)	571.0 ± 76.9	500	262.9 ± 49.5
		Water Recovery (%)	60 ~ 90	60	>87
		Major Components (AU\$/year) <sup>a</sup>	250,456	29,917	207,077
		Other Components (AU\$/year) <sup>a</sup>	26,806	2994	358
		<b>Subtotal (AU\$/year)</b>	<b>277,262</b>	<b>32,912</b>	<b>207,435</b>
O&M Cost, $C_{\text{O\&M}}$		Energy Cost (AU\$/year) <sup>c</sup>	59,422	123,301	99,532
		Acid Cost (AU\$/year) <sup>d</sup>	34,887	545,693	62,021
		Bleach Cost (AU\$/year)	2,243	2,243	2,243
		Antiscalant Cost (AU\$/year)	—	12,481	—
		Water Cost for Pure Water Cleaning (AU\$/year)	—	39,615	—
		$C_{\text{general O\&M}} \text{ (AU$/year)}$	<b>96,551</b>	<b>85,757</b>	<b>723,332</b>
Labour and Travel <sup>b</sup>		Essential Services Operator (AU\$/year)	2,756	2,756	13,780
		Technicians (AU\$/year)	34,344	17,172	68,688
		Travel and Chemical Transportation (AU\$/year) <sup>d</sup>	7,200	3,600	14,400
		$C_{\text{Labour \& Travel}} \text{ (AU$/year)}$	<b>44,300</b>	<b>23,528</b>	<b>85,844</b>
		<b>Subtotal (AU\$/year)</b>	<b>140,851</b>	<b>109,286</b>	<b>809,176</b>
		$C_{\text{capital}} + C_{\text{O\&M}} \text{ (AU$/year)}$	<b>418,113</b>	<b>386,548</b>	<b>842,088</b>
		<b>LCOW (AU\$/m<sup>3</sup>)</b>	<b>1.146</b>	<b>1.059</b>	<b>2.307</b>
					<b>1.335</b>

<sup>a</sup> Major components include RO elements and RO pressure vessels, MCDI modules and EDR stacks. Other components include process pumps, chemical dosing pumps and MCDI batteries. Further information is provided in SI Section S5a.

<sup>b</sup> Cost evaluation on general O&M and labour and travel was based on the information outlined in Section S5 of the SI.

<sup>c</sup> Energy consumption of specific components of MCDI systems in two operational modes and the simulated BWRO system can be found in Table S4 of the SI.

<sup>d</sup> Acid consumption of the MCDI system is the actual consumption observed over the trial, whereas the acid consumption of the simulated BWRO system is calculated based on WAVE™'s simulation results. Considering the significant larger amount of acid required for the simulated BWRO system 2 compared with other systems (as listed in SI Table S8), specific tank trailers could be needed to transport the acid, which will result in an additional AU\$0.037/m<sup>3</sup> onto the current LCOW estimation.

RCD-DNV operation were similar to those obtained during the CC-RCD-DPV operation, the ability to operate at a higher applied current led to an increase in the average TDS reduction by more than 60 mg/L. Additionally (and critically), the daily operating duration increased by approximately 8 h/day in CC-RCD-DNV, consequently resulting in a substantial increase in productivity of the unit.

The removal of major inorganic ions under the two CC operational modes was also examined over the long-term field trial. In terms of removal efficiency and ion selectivity, cations followed the order  $\text{Ca}^{2+} > \text{Mg}^{2+} > \text{K}^+ > \text{Na}^+$  while anions followed the order  $\text{SO}_4^{2-} >> \text{NO}_3^- > \text{Cl}^- > \text{F}^-$ , which is consistent with the results reported by other researchers that removal of small-multivalent ions is favoured over large-monovalent ions as a result of the differences in ionic charge and hydrated ion size. Additionally, an increase in selectivity of monovalent ions over divalent ions was observed on operating the MCDI unit in CC-RCD-DNV mode.

Lastly, energy and economic efficiency for brackish groundwater desalination in remote locations, where energy and maintenance resources are typically limited, was investigated in this study. The energy consumption of the MCDI pilot unit was 0.55 kWh/m<sup>3</sup> when operated in CC-RCD-DPV mode and 0.66 kWh/m<sup>3</sup> when operated in CC-RCD-DNV mode with these values significantly lower than that of a simulated BWRO system with the same production capacity of 20 m<sup>3</sup>/day. By scaling up the MCDI system to a capacity of 1000 m<sup>3</sup>/day, energy consumption is projected to decrease to 0.40 kWh/m<sup>3</sup> and 0.53 kWh/m<sup>3</sup> for CC-RCD-DPV and CC-RCD-DNV modes, respectively, which is comparable to the energy consumption of the EDR system (0.67 kWh/m<sup>3</sup>) and the simulated BWRO system (0.83 kWh/m<sup>3</sup>) with similar production capacities. Importantly, the LCOW of the scaled-up MCDI system (AU \$1.146/m<sup>3</sup> for CC-RCD-DPV and AU\$1.059/m<sup>3</sup> for CC-RCD-DNV modes respectively) is anticipated to be the lowest amongst all three water treatment technologies due particularly to the relatively simple maintenance and pre-treatment requirements of the MCDI units. The LCOW could be further reduced by integrating photovoltaic power supply and a more advanced energy recovery system with the MCDI system. In

summary, we conclude that MCDI is a water and cost-efficient means of desalinating brackish waters in small communities with flexibility in performance as a result of the range of different operating parameters and operational modes available. Investigations of trade-offs between the various MCDI performance metrics are required to further promote the upscaling of this promising water treatment technology.

Supplementary material is included and contains photographs of the pilot unit, details of optional operational modes, detailed MCDI performance data during operation in different operational modes, correlations between MCDI performance metrics and cycle time, details of simulated brackish water reverse osmosis (BWRO) systems, details of comparative energy and economic evaluation for MCDI, EDR and BWRO systems, preliminary results of trade-offs amongst different MCDI performance metrics, and two supplementary WAVE™ simulation reports.

#### CRediT authorship contribution statement

**Yunyi Zhu:** Data curation, Formal analysis, Investigation, Validation, Visualization, Writing – original draft. **Christopher Miller:** Data curation, Formal analysis, Investigation, Methodology, Visualization, Writing – review & editing. **Boyue Lian:** Conceptualization, Investigation, Methodology, Writing – review & editing. **Yuan Wang:** Funding acquisition, Investigation, Project administration, Resources, Supervision, Writing – review & editing, Conceptualization. **John Fletcher:** Conceptualization, Formal analysis, Funding acquisition, Investigation, Methodology, Resources, Supervision, Writing – review & editing. **Hang Zhou:** Formal analysis, Investigation, Methodology, Resources, Writing – review & editing. **Zhizhao He:** Investigation, Methodology, Writing – review & editing. **Shunzhi Lyu:** Methodology, Resources. **Megan Purser:** Funding acquisition, Investigation, Resources, Writing – review & editing. **Peter Jurachich:** Investigation, Methodology, Resources. **David Sweeney:** Investigation, Resources. **T. David Waite:** Conceptualization, Funding acquisition, Investigation, Methodology, Project administration, Resources, Supervision, Writing – review & editing.

## Declaration of competing interest

The authors declare that they have no known competing financial interests or personal relationships that could have appeared to influence the work reported in this paper.

## Data availability

Data will be made available on request.

## Acknowledgements

The authors gratefully acknowledge the generous support provided by Northern Territory Power and Water Corporation with respect to the construction, shipping, installation, commissioning and maintenance of the MCDI trial unit. The support of Catherine Vero in the early stages of this project is also acknowledged. Yunyi Zhu is supported by an Australian Government Research Training Program (RTP) Scholarship.

## Supplementary materials

Supplementary material associated with this article can be found, in the online version, at [doi:10.1016/j.watres.2024.121413](https://doi.org/10.1016/j.watres.2024.121413).

## References

- Al-Obaidi, M.A., Alsarayreh, A.A., Bdour, A., Jassam, S.H., Rashid, F.L., Mujtaba, I.M., 2023. Simulation and optimisation of a medium scale reverse osmosis brackish water desalination system under variable feed quality: energy saving and maintenance opportunity. Desalination 565, 116831. <https://doi.org/10.1016/j.desal.2023.116831>.
- Anderson, M.A., Cudero, A.L., Palma, J., 2010. Capacitive deionization as an electrochemical means of saving energy and delivering clean water. Comparison to present desalination practices: will it compete? *Electrochim. Acta* 55, 3845–3856. <https://doi.org/10.1016/j.electacta.2010.02.012>.
- Australian Government Geoscience Australia, 2023. *Groundwater Use*.
- Bales, C., Lian, B., Zhu, Y., Zhou, H., Wang, Y., Fletcher, J., Waite, T.D., 2023. Photovoltaic powered operational scale Membrane Capacitive Deionization (MCDI) desalination with energy recovery for treated domestic wastewater reuse. Desalination 559, 116647. <https://doi.org/10.1016/j.desal.2023.116647>.
- Biesheuvel, P.M., van der Wal, A., 2010. Membrane capacitive deionization. *J. Memb. Sci.* 346, 256–262. <https://doi.org/10.1016/j.memsci.2009.09.043>.
- Biesheuvel, P.M., Zhao, R., Porada, S., van der Wal, A., 2011. Theory of membrane capacitive deionization including the effect of the electrode pore space. *J. Colloid Interface Sci.* 360, 239–248. <https://doi.org/10.1016/j.jcis.2011.04.049>.
- Cerón, M.R., Aydin, F., Hawks, S.A., Oyarzun, D.I., Loeb, C.K., Deinhart, A., Zhan, C., Pham, T.A., Stadermann, M., Campbell, P.G., 2020. Cation selectivity in capacitive deionization: elucidating the role of pore size, electrode potential, and ion dehydration. *ACS Appl. Mater. Interfaces* 12, 42644–42652. <https://doi.org/10.1021/acsmami.0c07903>.
- Chen, L., Yin, X., Zhu, L., Qiu, Y., 2018a. Energy recovery and electrode regeneration under different charge/discharge conditions in membrane capacitive deionization. Desalination 439, 93–101. <https://doi.org/10.1016/j.desal.2018.04.012>.
- Chen, L., Yin, X., Zhu, L., Qiu, Y., 2018b. Energy recovery and electrode regeneration under different charge/discharge conditions in membrane capacitive deionization. Desalination 439, 93–101. <https://doi.org/10.1016/j.desal.2018.04.012>.
- Chheang, M., Hongprasith, N., Ratanatawanate, C., Lohwacharin, J., 2022. Effects of chemical cleaning on the ageing of polyvinylidene fluoride microfiltration and ultrafiltration membranes fouled with organic and inorganic matter. *Membranes (Basel)* 12. <https://doi.org/10.3390/membranes12030280>.
- Dlugolecki, P., van der Wal, A., 2013. Energy recovery in membrane capacitive deionization. *Environ. Sci. Technol.* 47, 4904–4910. <https://doi.org/10.1021/es3053202>.
- Duranceau, S.J., 2009. Desalination post-treatment considerations. *Florida Water Res.our.* **4**, 1–18.
- Dykstra, J.E., Porada, S., van der Wal, A., Biesheuvel, P.M., 2018. Energy consumption in capacitive deionization – constant current versus constant voltage operation. *Water Res.* 143, 367–375. <https://doi.org/10.1016/j.watres.2018.06.034>.
- Gamaethiralalage, J.G., Singh, K., Sahin, S., Yoon, J., Elimelech, M., Suss, M.E., Liang, P., Biesheuvel, P.M., Zornetta, R.L., de Smet, L.C.P.M., 2021. Recent advances in ion selectivity with capacitive deionization. *Energy Environ. Sci.* 14, 1095–1120. <https://doi.org/10.1039/D0EE03145C>.
- Hassanvand, A., Chen, G.Q., Webley, P.A., Kentish, S.E., 2018. A comparison of multicomponent electrosorption in capacitive deionization and membrane capacitive deionization. *Water Res.* 131, 100–109. <https://doi.org/10.1016/j.watres.2017.12.015>.
- Hassanvand, A., Wei, K., Talebi, S., Chen, G.Q., Kentish, S.E., 2017. The role of ion exchange membranes in membrane capacitive deionisation. *Membranes (Basel)*. <https://doi.org/10.3390/membranes7030054>.
- Hawks, S.A., Cerón, M.R., Oyarzun, D.I., Pham, T.A., Zhan, C., Loeb, C.K., Mew, D., Deinhart, A., Wood, B.C., Santiago, J.G., Stadermann, M., Campbell, P.G., 2019a. Using ultramicroporous carbon for the selective removal of nitrate with capacitive deionization. *Environ. Sci. Technol.* 53, 10863–10870. <https://doi.org/10.1021/acs.est.9b01374>.
- Hawks, S.A., Ramachandran, A., Porada, S., Campbell, P.G., Suss, M.E., Biesheuvel, P.M., Santiago, J.G., Stadermann, M., 2019b. Performance metrics for the objective assessment of capacitive deionization systems. *Water Res.* 152, 126–137. <https://doi.org/10.1016/j.watres.2018.10.074>.
- He, Z., Li, Y., Wang, Y., Miller, C.J., Fletcher, J., Lian, B., Waite, T.D., 2023. Insufficient desorption of ions in constant-current membrane capacitive deionization (MCDI): problems and solutions. *Water Res.* 242, 120273. <https://doi.org/10.1016/j.watres.2023.120273>.
- He, Z., Liu, S., Lian, B., Fletcher, J., Bales, C., Wang, Y., Waite, T.D., 2021. Optimization of constant-current operation in membrane capacitive deionization (MCDI) using variable discharging operations. *Water Res.* 204, 117646. <https://doi.org/10.1016/j.watres.2021.117646>.
- Hou, C.-H., Huang, C.-Y., 2013. A comparative study of electrosorption selectivity of ions by activated carbon electrodes in capacitive deionization. *Desalination* 314, 124–129. <https://doi.org/10.1016/j.desal.2012.12.029>.
- Kang, J., Kim, T., Jo, K., Yoon, J., 2014. Comparison of salt adsorption capacity and energy consumption between constant current and constant voltage operation in capacitive deionization. *Desalination* 352, 52–57. <https://doi.org/10.1016/j.desal.2014.08.009>.
- Kim, D.I., Dorji, P., Gwak, G., Phuntsho, S., Hong, S., Shon, H., 2019. Reuse of municipal wastewater via membrane capacitive deionization using ion-selective polymer-coated carbon electrodes in pilot-scale. *Chem. Eng. J.* 372, 241–250. <https://doi.org/10.1016/j.cej.2019.04.156>.
- Kim, N., Lee, J., Kim, S., Hong, S.P., Lee, C., Yoon, J., Kim, C., 2020. Short review of multichannel membrane capacitive deionization: principle, current status, and future prospect. *Appl. Sci.* <https://doi.org/10.3390/app10020683>.
- Lamei, A., van der Zaag, P., von Münch, E., 2008. Basic cost equations to estimate unit production costs for RO desalination and long-distance piping to supply water to tourism-dominated arid coastal regions of Egypt. *Desalination* 225, 1–12. <https://doi.org/10.1016/j.desal.2007.08.003>.
- Lee, J.-H., Choi, J.-H., 2012. The production of ultrapure water by membrane capacitive deionization (MCDI) technology. *J. Memb. Sci.* 409–410, 251–256. <https://doi.org/10.1016/j.memsci.2012.03.064>.
- Luong, V.T., Cañas Kurz, E.E., Hellriegel, U., Dinh, D.N., Tran, H.T., Figoli, A., Gabriele, B., Luu, T.L., Hoinkis, J., 2023. Modular desalination concept with low-pressure reverse osmosis and capacitive deionization: performance study of a pilot plant in Vietnam in comparison to seawater reverse osmosis. *J. Environ. Manage.* 329, 117078. <https://doi.org/10.1016/j.jenvman.2022.117078>.
- McNair, R., Szekely, G., Dryfe, R.A.W., 2021. Ion-exchange materials for membrane capacitive deionization. *ACS ES&T Water* 1, 217–239. <https://doi.org/10.1021/acsestwater.0c00123>.
- Mei, Y., Yao, Z., Ji, L., Toy, P.H., Tang, C.Y., 2018. Effects of hypochlorite exposure on the structure and electrochemical performance of ion exchange membranes in reverse electrodialysis. *J. Memb. Sci.* 549, 295–305. <https://doi.org/10.1016/j.memsci.2017.12.016>.
- Mossad, M., Zou, L., 2012. A study of the capacitive deionisation performance under various operational conditions. *J. Hazard. Mater.* 213–214, 491–497. <https://doi.org/10.1016/j.jhazmat.2012.02.036>.
- National Association of Testing Authorities, 2024. *Water Chemistry Laboratory*.
- National Health and Medical Research Council, 2011. *Australian Drinking Water Guidelines*.
- Nightingale, E.R.J., 1959. Phenomenological theory of ion solvation. effective radii of hydrated ions. *J. Phys. Chem.* 63, 1381–1387. <https://doi.org/10.1021/j150579a011>.
- Pan, S.-Y., Haddad, A.Z., Kumar, A., Wang, S.-W., 2020. Brackish water desalination using reverse osmosis and capacitive deionization at the water-energy nexus. *Water Res.* 183, 116064. <https://doi.org/10.1016/j.watres.2020.116064>.
- Papavinasam, S., 2014. Chapter 14 - Management. In: Papavinasam, S. (Ed.), *Corrosion Control in the Oil and Gas Industry*. Gulf Professional Publishing, Boston, pp. 841–918. <https://doi.org/10.1016/B978-0-12-397022-0-00014-5>.
- Pearson, J.L., Michael, P.R., Ghaffour, N., Missimer, T.M., 2021. Economics and energy consumption of brackish water reverse osmosis desalination: innovations and impacts of feedwater quality. *Membranes*. <https://doi.org/10.3390/membranes11080616>.
- Porada, S., Zhao, R., Van Der Wal, A., Presser, V., Biesheuvel, P.M., 2013. Review on the science and technology of water desalination by capacitive deionization. *Prog. Mater. Sci.* 58, 1388–1442. <https://doi.org/10.1016/j.pmatsci.2013.03.005>.
- Qu, Y., Campbell, P.G., Gu, L., Knipe, J.M., Dzenitis, E., Santiago, J.G., Stadermann, M., 2016. Energy consumption analysis of constant voltage and constant current operations in capacitive deionization. *Desalination* 400, 18–24. <https://doi.org/10.1016/j.desal.2016.09.014>.
- Ramachandran, A., Hemmatifar, A., Hawks, S.A., Stadermann, M., Santiago, J.G., 2018. Self similarities in desalination dynamics and performance using capacitive deionization. *Water Res.* 140, 323–334. <https://doi.org/10.1016/j.watres.2018.04.042>.
- Ramachandran, A., Oyarzun, D.I., Hawks, S.A., Stadermann, M., Santiago, J.G., 2019. High water recovery and improved thermodynamic efficiency for capacitive

- deionization using variable flowrate operation. *Water Res.* 155, 76–85. <https://doi.org/10.1016/j.watres.2019.02.007>.
- Sedighi, M., Behvand Usefi, M.M., Ismail, A.F., Ghasemi, M., 2023. Environmental sustainability and ions removal through electrodialysis desalination: operating conditions and process parameters. *Desalination* 549, 116319. <https://doi.org/10.1016/j.desal.2022.116319>.
- Seo, S.-J., Jeon, H., Lee, J.K., Kim, G.-Y., Park, D., Nojima, H., Lee, J., Moon, S.-H., 2010. Investigation on removal of hardness ions by capacitive deionization (CDI) for water softening applications. *Water Res.* 44, 2267–2275. <https://doi.org/10.1016/j.watres.2009.10.020>.
- Sharan, P., Yoon, T.J., Jaffe, S.M., Ju, T., Currier, R.P., Findikoglu, A.T., 2021. Can capacitive deionization outperform reverse osmosis for brackish water desalination? *Clean. Eng. Technol.* 3, 100102 <https://doi.org/10.1016/j.clet.2021.100102>.
- Shen, Y.Y., Sun, S.H., Tsai, S.W., Chen, T.H., Hou, C.H., 2021. Development of a membrane capacitive deionization stack for domestic wastewater reclamation: a pilot-scale feasibility study. *Desalination* 500, 114851. <https://doi.org/10.1016/j.desal.2020.114851>.
- Son, M., Yoon, N., Park, S., Abbas, A., Cho, K.H., 2023. An open-source deep learning model for predicting effluent concentration in capacitive deionization. *Sci. Total Environ.* 856, 159158 <https://doi.org/10.1016/j.scitotenv.2022.159158>.
- Suss, M., Porada, S., Sun, X., Biesheuvel, M., Yoon, J., Presser, V., 2015. Water desalination via capacitive deionization: what is it and what can we expect from it? *Energy Environ. Sci.* 8 <https://doi.org/10.1039/C5EE00519A>.
- Tan, C., He, C., Fletcher, J., Waite, T.D., 2020. Energy recovery in pilot scale membrane CDI treatment of brackish waters. *Water Res.* 168, 115146 <https://doi.org/10.1016/j.watres.2019.115146>.
- Tan, C., He, C., Tang, W., Kovalsky, P., Fletcher, J., Waite, T.D., 2018. Integration of photovoltaic energy supply with membrane capacitive deionization (MCDI) for salt removal from brackish waters. *Water Res.* 147, 276–286. <https://doi.org/10.1016/j.watres.2018.09.056>.
- Tang, W., He, D., Zhang, C., Kovalsky, P., Waite, T.D., 2017. Comparison of Faradaic reactions in capacitive deionization (CDI) and membrane capacitive deionization (MCDI) water treatment processes. *Water Res.* 120, 229–237. <https://doi.org/10.1016/j.watres.2017.05.009>.
- van Limpert, B., van der Wal, A., 2014. Water and chemical savings in cooling towers by using membrane capacitive deionization. *Desalination* 342, 148–155. <https://doi.org/10.1016/j.desal.2013.12.022>.
- Vanysek, P., 1993. Ionic conductivity and diffusion at infinite dilution. CRC hand B. *Chem. Phys.* 5–92.
- Wang, L., Lin, S., 2019. Mechanism of selective ion removal in membrane capacitive deionization for water softening. *Environ. Sci. Technol.* 53, 5797–5804. <https://doi.org/10.1021/acs.est.9b00655>.
- Wang, L., Lin, S., 2018. Membrane capacitive deionization with constant current vs constant voltage charging: which is better? *Environ. Sci. Technol.* 52, 4051–4060. <https://doi.org/10.1021/acs.est.7b06064>.
- World Health Organization, 2024. Drinking-Water.
- Xu, P., Drewes, J.E., Heil, D., Wang, G., 2008. Treatment of brackish produced water using carbon aerogel-based capacitive deionization technology. *Water Res.* 42, 2605–2617. <https://doi.org/10.1016/j.watres.2008.01.011>.
- Xu, X., Ness, J.E., Miara, A., Sitterley, K.A., Talmadge, M., O'Neill, B., Coughlin, K., Akar, S., Edirisoriya, E.M.N.T., Kurup, P., Rao, N., Macknick, J., Stokes-Draut, J.R., Xu, P., 2022. Analysis of brackish water desalination for municipal uses: case studies on challenges and opportunities. *ACS ES&T Eng* 2, 306–322. <https://doi.org/10.1021/acestengg.1c00326>.
- Yao, Q., Tang, H.L., 2017. Effect of desorption methods on electrode regeneration performance of capacitive deionization. *J. Environ. Eng.* 143, 4017047 [https://doi.org/10.1061/\(ASCE\)EE.1943-7870.0001245](https://doi.org/10.1061/(ASCE)EE.1943-7870.0001245).
- Zhang, W., Mossad, M., Zou, L., 2013. A study of the long-term operation of capacitive deionisation in inland brackish water desalination. *Desalination* 320, 80–85. <https://doi.org/10.1016/j.desal.2013.04.010>.
- Zhao, R., Biesheuvel, P.M., van der Wal, A., 2012a. Energy consumption and constant current operation in membrane capacitive deionization. *Energy Environ. Sci.* 5, 9520–9527. <https://doi.org/10.1039/C2EE21737F>.
- Zhao, R., Porada, S., Biesheuvel, P.M., van der Wal, A., 2013. Energy consumption in membrane capacitive deionization for different water recoveries and flow rates, and comparison with reverse osmosis. *Desalination* 330, 35–41. <https://doi.org/10.1016/j.desal.2013.08.017>.
- Zhao, R., van Soestbergen, M., Rijnaarts, H.H.M., van der Wal, A., Bazant, M.Z., Biesheuvel, P.M., 2012b. Time-dependent ion selectivity in capacitive charging of porous electrodes. *J. Colloid Interface Sci.* 384, 38–44. <https://doi.org/10.1016/j.jcis.2012.06.022>.
- Zhou, H., Tan, C., Fletcher, J., 2018. Lossless bi-directional current sense circuit for low-voltage high-current DC/DC converters. In: IECON 2018 - 44th Annual Conference of the IEEE Industrial Electronics Society, pp. 1305–1308. <https://doi.org/10.1109/IECON.2018.8591710>.